UNIVERSITÀ
DEGLI STUDI
DI PADOVA

DIPARTIMENTO
DI INGEGNERIA
DELL'INFORMAZIONE

DIPARTIMENTO DI INGEGNERIA DELL'INFORMAZIONE

CORSO DI LAUREA MAGISTRALE IN BIOINGEGNERIA

Implementation of a new TMS-EEG source reconstruction model using fMRI-DTI template as a prior: a comparative study with the state of the art.

Relatore: Prof. Veronese Mattia
Correlatrici: Dr.ssa Bortoletto Marta
Dr.ssa Stango Antonietta

Laureanda: Cinelli Sara

ANNO ACCADEMICO 2023-2024

Data di laurea 04/12/2024

Index

Abbreviations

BEM Boundary element method

BOLD Blood oxygen level dependent

CC Corpus callosum

CEN Central executive network

CNS Central nervous system

CSF Cerebrospinal fluid

DAN Dorsal attention network

DMN Default mode network

EEG Electroencephalography

FDM Finite difference method

FEM Finite element method

FVM Finite volume method

GM Grey matter

fMRI Functional magnetic resonance imaging

M1 cortex Primary motor cortex

MN Minimum norm

MRI Magnetic resonance imaging

MS Multiple sclerosis

PNS Peripherical nervous system

PSP Post synaptic potential

RSN Resting state network

SNR Signal to noise ratio

TMS Transcranial magnetic stimulation

VAN Ventral attention network

WM White matter

Abstract

This study was conducted at the Neurophysiology Laboratory, IRCCS Centro San Giovanni di Dio Fatebenefratelli in Brescia. The objective involved the implementation and evaluation of a new method for reconstructing transcranial evoked potential sources. In contrast to traditional methods, the new approach integrates a priori information on grey matter regions structurally connected to the primary motor cortex, which is stimulated during the transcranial magnetic stimulation experiment. Due to technical constraints, it was not possible to use individual tractography data to reconstruct the networks of connections; therefore, an fMRI-DTI template of the sensorimotor network of the right hand in the resting state was adopted.

The pilot study implemented two distinct approaches:

- "**A posteriori**" method (traditional method): includes all grey matter in the source model and only then focuses on areas structurally connected to primary motor cortex.
- "**A priori**" method (new method): includes only the areas structurally linked with primary motor cortex directly in the source model.

Analyses focused on four main aspects: (1) **verification of the 'A posteriori' method**, which confirmed the major activity in the network areas; (2) **evaluation of the main effect of the methods**, which showed similar performance within the brain network; (3) **evaluation of the main effect of the ROIs** (Region Of Interest), identifying significant differences between them; (4) **evaluation of the ROI-method interaction**, which revealed differences in the cerebellum results with the 'A priori' method.

The 'A priori' method proved to be more sensitive in detecting the activation of cerebellar regions than the traditional method. Although the overall activation of the sensorimotor network was similar, the new approach showed a greater ability to localise specific cerebellar activations. This result underlines the potential of the 'A priori' method to improve understanding of brain networks and develop more targeted interventions, particularly useful for patients with alterations in anatomical structure or patterns of brain connectivity.

Sommario

Questo studio è stato condotto presso il Laboratorio di Neurofisiologia dell'IRCCS Centro San Giovanni di Dio Fatebenefratelli a Brescia. L'obiettivo prevedeva l'implementazione e la valutazione di un nuovo metodo di ricostruzione delle sorgenti dei potenziali evocati transcranici. A differenza dei metodi tradizionali, il nuovo approccio integra informazioni a priori sulle regioni di sostanza grigia strutturalmente connesse alla corteccia motoria primaria, stimolata durante l'esperimento con la stimolazione magnetica trancranica. Per vincoli tecnici, non è stato possibile utilizzare dati di trattografia individuale per ricostruire le rete di connessioni; si è quindi adottato un template fMRI-DTI del network sensorimotorio della mano destra in stato di riposo. Lo studio pilota ha implementato due approcci distinti:

- Metodo **"A posteriori"** (metodo tradizionale):include tutta la materia grigia nel modello di sorgente e solo successivamente si focalizza sulle aree strutturalmente connesse alla corteccia motoria primaria.
- Metodo **"A priori"** (nuovo metodo): integra direttamente nel modello di sorgente solo le aree connesse strutturalmente con la corteccia motoria primaria.

Le analisi si sono concentrate su quattro aspetti principali: (1) **verifica del metodo "A posteriori**", che ha confermato una maggiore attività nelle aree del network; (2) **valutazione dell'effetto principale dei metodi**, che ha mostrato performance simili all'interno del network cerebrale; (3) **valutazione dell'effetto principale delle ROIs** (Regioni di Interesse), individuando differenze significative tra queste; (4) **valutazione interazione ROI-metodo**, che ha rivelato differenze nei risultati prevenienti dal cervelletto con il metodo "A priori".

Il metodo "A priori" si è dimostrato più sensibile nel rilevare l'attivazione delle regioni cerebellari rispetto al metodo tradizionale. Sebbene l'attivazione complessiva del network sensomotorio sia risultata simile, il nuovo approccio ha evidenziato una maggiore capacità di localizzare specifiche attivazioni cerebellari. Questo risultato sottolinea il potenziale del metodo "A priori" per migliorare la comprensione delle reti cerebrali e sviluppare interventi più mirati, particolarmente utili per pazienti con alterazioni nella struttura anatomica o nei pattern di connettività cerebrale.

1. Introduction

1.1 The nervous system

The nervous system is the complex and highly specialized network which is responsible to control the exchange of information between the body and the external environment [1]. It is composed by specialized cells and tissues which are build to permit the transmission of signals between the different parts of the body. The purpose of the following section is to give the essential knowledge regarding the neuroanatomy and the neurophysiology for the understanding of this thesis.

1.1.1 Basics of neuroanatomy

The neuron is the functional unit of the nervous system [1]. In the following figure it is shown a simple representation of this base unit which includes the dendrites, the soma and the axon. The dendrites and the axon are cell extensions, which receives respectively the information from the outside of the cell and transport the output signal to other cells. The soma, or cell body, is the main centre of the cell where the information is integrated, and an output signal is created. This output, as it is shown in the figure 1.1.1, follows a determined direction going along the axon towards the axon terminal. The axon is surrounded by the myelin sheath, which is composed by different layers of this particular substance, the myelin, whose function is the support and the conduction of the signal. The presence of the myelin is not homogeneous, but this occurs with 1-1.5 mm portions alternating with bare spots, called nodes of Ranvier.

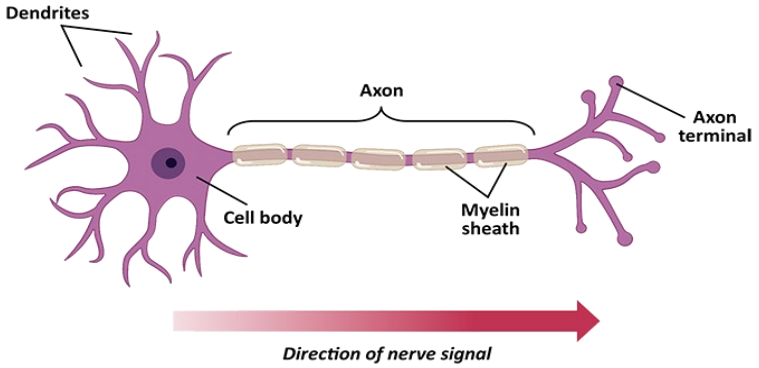

Figure 1.1.1 Structure of the neuron (NIH, 2024)

The presence of the myelin guarantees the high transmission speed of the nerve impulses.

For this reason, the loss of this sheat can lead to serious problems, like in demyelinating diseases [1]. In this context, the **multiple sclerosis** (MS) is the most known and most common disease of this type. It is a neurodegenerative autoimmune disease whose main sign is the loss of the myelin, i.e. white matter (WM), that leads to the creation of scar tissue, called sclerosis, visible with the magnetic resonance imaging (MRI).
The early symptoms mainly includes vision problems, muscle weakness, clumsiness and dizziness, and depend on the severity of the inflammation as well as the presence of scar tissues [2].
The figure 1.1.2 shows the prevalence of this disease in the year 2023, which counts 2.9 million people, while in 2013 the number was 2.3 million.

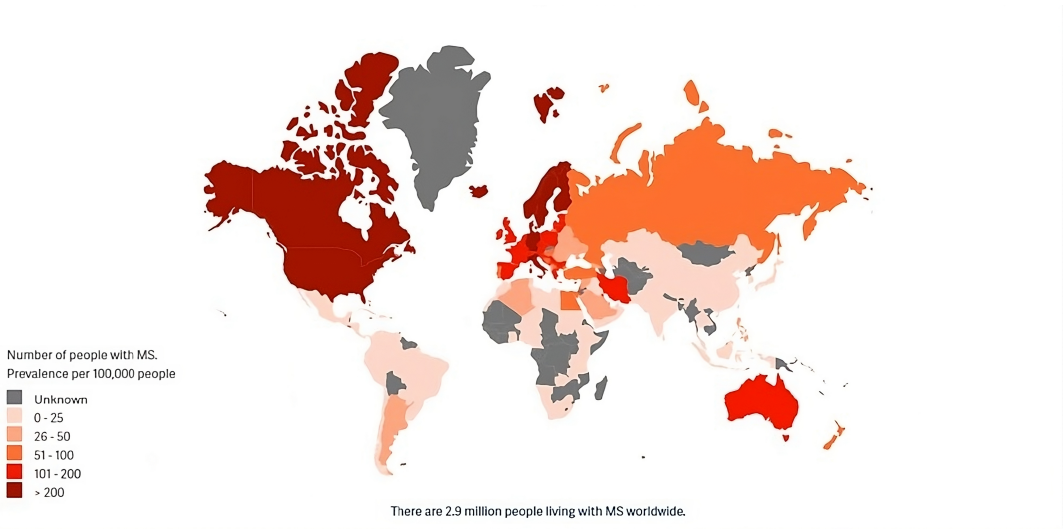

Figure 1.1.2 Prevalence of MS (MSIF, 2024)

Coming back to the anatomy of the neuron, it is essential to talk about the synapse: this term refers to the communication site between the neurons, in particular to the space between the axon terminals of the presynaptic neuron and the dendrites of the postsynaptic neuron. The synapses can be electrical or chemical, depending on the way the signal is transmitted. In the figure 1.1.2 there is the representation of a chemical one where the neurotransmitters, the chemical substances exchanged, represent the conversion of the electrical impulse. These molecules are contained in vesicles which are released from the axon terminal to reach the receptors on the postsynaptic neuron. Neurotransmitters, such as acetylcholine, glutamate, GABA, serotonin, and dopamine, play essential roles in neural communication by transmitting signals across synapses. The strength of a signal is often associated with the amount of neurotransmitter released, with stronger signals resulting in greater quantities of these molecules being released and subsequently detected by receptor neurons.

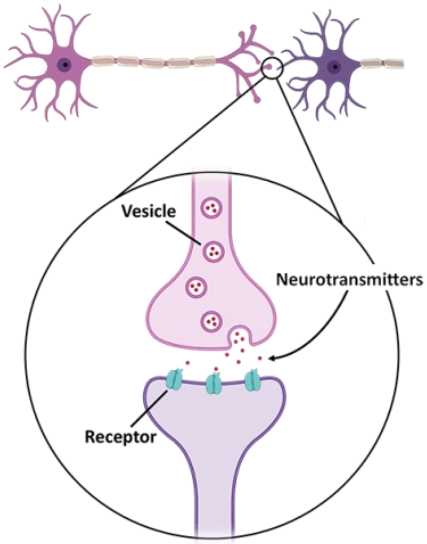

Figure 1.1.3 The synapse (NIH, 2024)

Of course, there are other cells which have a fundamental role in the nervous system, but for this thesis their description can be neglected.

Moving to a larger prospective, it is possible to give an overview of the central nervous system (CNS) and especially on the brain. The nervous system is divided into two parts: the CNS and the peripheral nervous system (PNS) [1]. The first one is composed by the brain and the spinal cord; the second is composed by the nerves that branch off from the brain and the spinal cord and extend to all parts of the body.

A macroscopic classification that is useful to highlight is the division of the CNS in grey matter (GM) and WM, based on the different colouring presented by the neuronal tissue. The first one refers to each part of the neuron where there is no myelin, i.e. the soma, the dendrites and the terminal part of the axons; the second one refers to the opposite, i.e. the axons. A clear representation of this is depicted in figure 1.1.5.

The brain is surrounded by the cranium and the spinal cord is protected by the vertebrae. In addition to the bone, the CNS is surrounded by the meninges and the cerebrospinal fluid.

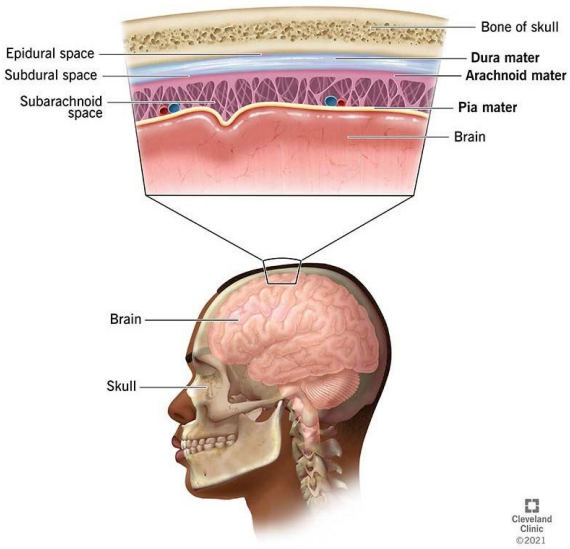

Figure 1.1.4 The brain

In the figure 1.1.4 there is the schematic representation of the layers that surrounds the brain. In particular there are the meninges, the pia mater, the arachnoid mater and the dura mater, which are three membranes composed by connective tissue. These are important because of the support and nutrition function for the brain. The last two layers are the bone and the scalp. From the figure it is clear the presence of three spaces between the bone and the meninges and between the meninges themselves. In particular the subarachnoid space is filled by the cerebrospinal fluid (CSF), and it surrounds the spinal cord as well. This fluid is colourless and odourless and it has a nutrition, support and waste cleaning function.

The brain is the main component of the CNS and it is divided into cerebrum, cerebellum and brainstem. The cerebrum is the largest part of the brain, it is composed of two symmetric hemispheres (right and left) and it is responsible for handling sensorial information and high cognitive functions like reasoning, managing emotions and control of movement. The cerebellum is located under the cerebrum and it is important for the coordination of muscle movements and balance. The brainstem connects the brain with the spinal cord and it is crucial for many automatic functions such as the regulation of breathing, heart rate, body temperature, digestion and sleep cycles.

The outermost layer of the brain is called cerebral cortex, which is known as the GM of the brain, and it is the centre of the conscious mind [1]. It has a thickness of 2-4 mm and it contains approximately 75% of the neuron cell bodies of the nervous system.

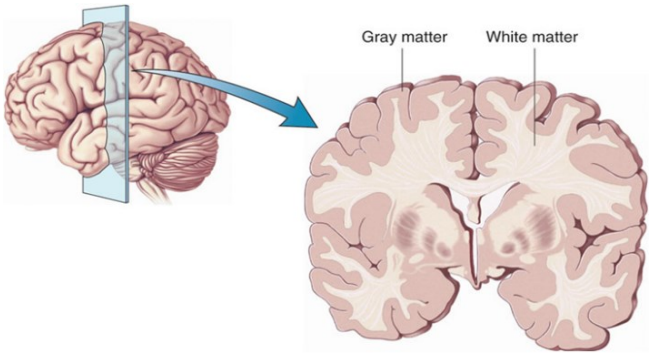

Figure 1.1.5 Coronal section of the brain (NIH, 2024)

The areas of the cortex of each hemisphere can be categorised into three types: the sensorial area, the motor area and the association area. Even if the cerebrum is symmetric, with sensorial and motor areas which controls the opposite part of the body, some cognitive and compartmental function are not symmetric. Infact, the linguistic and reasoning faculties tend to be localized in the left hemisphere, while the right one is specialized imagination and creativity. These functional areas does not acts individually, but every action borns from the activation of the different part of the cortex [3].

In particular, the cerebral cortex has been classified into four lobes according to the cranial bone under which they are located: frontal, parietal, temporal and occipital.

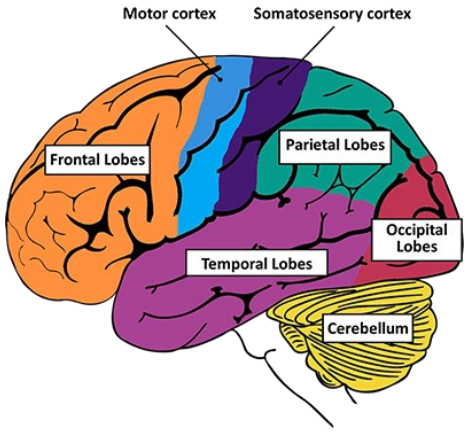

Figure 1.1.6 Functional divisions of the brain (NIH, 2024)

In the back portion of each frontal lobe there is a motor cortex, which includes the primary motor cortex (M1) responsible for planning and execution of voluntary movements. The forward part of the parietal lobes is the somatosensory cortex, which receives sensory information from the body.

The WM that enables the connection between neurons constitutes the corpus callosum (CC). In particular, this ensures interhemispheric connectivity, as it is the largest interhemispheric commissure in the human brain composed of about 200 million [4]. The corticospinal tract (CST) is the major neuronal pathway that controls voluntary movements [5] .

Getting even more specific, it is important to introduce the concept of resting state network (RSN), groups of brain regions which exhibit functionally connected activity at rest, i.e. not engaged in any specific task [6], [7]. These networks are identified using functional magnetic resonance imaging (fMRI) in which the blood oxygen level dependent (BOLD) signal is analysed. The primary seven RSN typically identified in the human brain are [8]:

1. Default Mode Network (DMN): self-referencial thinking and mind-wandering.
2. Salience Network: detecting important stimuli;
3. Central Executive Network (CEN): working memory and decision-making;
4. Dorsal Attention Network (DAN): goal-directed attention and visual processing;
5. Ventral Attention Network (VAN): attention reorienting;
6. Somatomotor Network: planning and execution of movement;
7. Visual Network: visual perception and processing.

There exists other division which includes more RSN, like in the paper of [9], where an atlas of 30 RSNs has been created. In particular there have been individualized the regions related to the left and right hand inside the sensorimotor network.

1.1.2 Basics of neurophysiology

The nervous system has the peculiar capacity to produce and propagates rapidly the electrical signal generated as the answer to a stimulus [1].

In the previous paragraph it has been introduced the concept of synapse, referring to the electrical and the chemical one. In the first one, the conduction of the electrical impulse passes directly from the presynaptic neuron to the postsynaptic one, without the use of neurotransmitters.

The most interesting is the chemical synapse, which it is briefly described in the next paragraph.

One of the first concept that has to be introduced is the membrane potential, a difference of electric charge between inside and outside of the neuron. At rest it measures -70 mV due to the unequal distribution of sodium (Na^+) and potassium (K^+) ions. This equilibrium is maintained by the sodium-potassium pump (Na^+/K^+-ATPase). A significant change in the membrane potential (until -55mV) generates a **action potential** (AP), is a rapid and transitory change in the membrane potential which originates in the soma, and it propagates in the axon towards other cells.

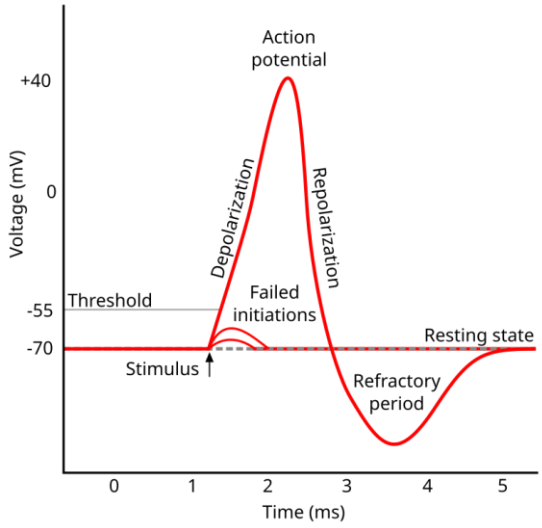

Figure 1.1.7 Potential action (NIH, 2024)

When an AP reaches the terminal axon, there is the conversion of the electrical signal into a chemical one, whit the release of a well determined amount of neurotransmitter. When this stimulus reaches the postsynaptic neuron, there is the reconversion into an electrical signal, a **post synaptic potential** (PSP) is created. The PSP is a temporary change inmembrane potential of the post synaptic neuron that can depolarize (excitatory PSD) or repolarize the membrane (inhibitory PSD).

Differently from the AP, the creation of a PSD does not require the exceeding of a threshold to originate it: infact, the PSD is a graduated potential which means it can be spatially and temporally summed, and the result will determine the trigger of AP or not. For this reason, the PSDs are fundamental for the integration of the information in the nervous system. The PSD of pyramidal cells in the cerebral cortex are the one measured with the electroencephalography (EEG).

The conduction of the AP through the axon is guaranteed by the presence of the myelin: if the sheath is damaged or disrupted for some reason, e.g. demyelinating disease or trauma, the conduction of the signal is slowed down.

1.1.3 Brain connectivity

The focus can be directed towards the concept of brain connectivity, taking into account the spatiotemporal dynamics of the neuronal communication. Infact, the human brain is considered a complex network in which hundreds of brain regions are interconnected via axonal pathways [10]. The concepts of network and the activation of different interconnected areas have been adopted in [11] and it is noteworthy for this thesis. In particular, it is important to talk about structural connectivity and functional connectivity. The first one refers to the anatomical connections between brain regions by WM fibres; the second one includes the concept of statistical dependence between those regions. A measure of these connections can be assessed by the tractography and the EEG/fMRI, respectively.

It is known that structural connectivity shapes functional connectivity [12]: this fact justifies the use of combined electroencephalography and tractography to study the link between the two. In figure 1.1.8 there is the illustration of the different recording modalities.

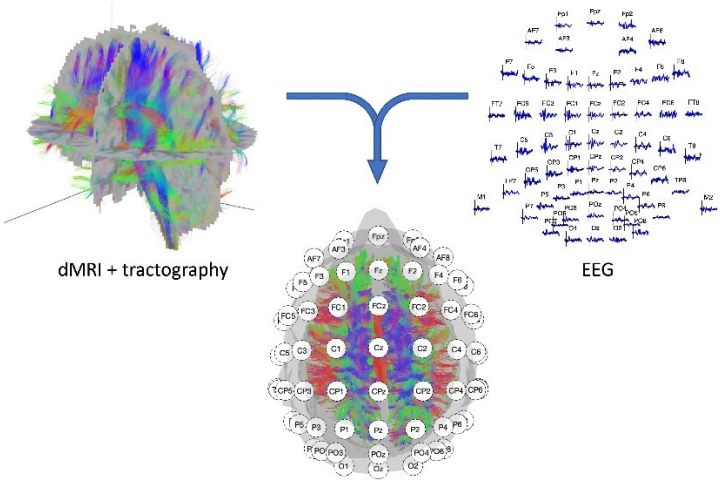

Figure 1.1.8: (Left top panel) dMRI recording with resulting fiber tracts. (Right top panel) 64-channel EEG signal with electrode layout conform the 10–20 systematic. (Middle lower panel) EEG/dMRI combination to explore the link between structural and functional connectivity. [13]

There is also a third type of connectivity, the effective connectivity, which refers to the causal interaction between brain regions and it can be detected by the combined use of TMS-EEG.

1.2 Co-registration TMS-EEG

The combined use of transcranial magnetic stimulation and electroencephalography (TMS-EEG) has already been defined as the state of the art to investigate the causal relationship between brain regions in humans, i.e. the effective connectivity [14], [15]. In the following sections a brief description on both the single techniques and the combined one is given.

1.2.1 Transcranial magnetic stimulation

The TMS is a type of non-invasive brain stimulation method which is used in humans [16]. In the 20th century, the first experimentation with the stimulation of the motor cortex on animals took place [17]. The 1985 instead was the year of the first experiment with this technology in humans [18].

This technology has different application, like experimental and investigational but also therapeutic ones, e.g. cure of major depressive disorder, obsessive-compulsive disorder and migraine [19].

The mechanism of action includes the principles of the electro-magnetic induction. When an electric current flows through the coil, a magnetic field is generated, which induces the creation of an electric field and the resulting stimulation of the neuronal tissue [19]. The depth of stimulation can vary from 2 to 4 cm below the cortical surface, so only the superficial brain structure are stimulated [20].

The main interesting application site is the motor cortex, as it can be used to study the pyramidal tract projecting on spinal motoneurons, also termed corticospinal tract [21]. Motor neuron activation leads to a contraction in the target muscles evoking a motor-evoked potential (MEP) on the electromyography (EMG) [22].

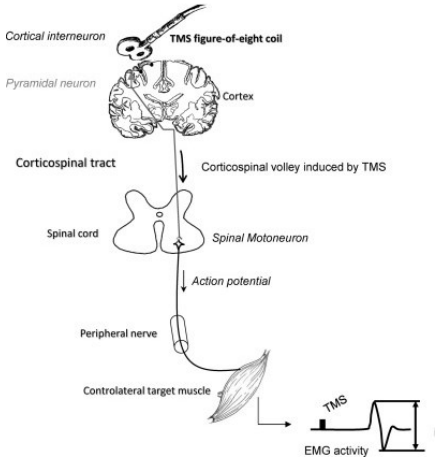

Figure 1.2.1 Scheme of mechanism of action of TMS of the motor cortex, (Klomjai et al., 2015)

1.2.2 Electroencephalography

The electroencephalography (EEG) is the non-invasive measurement of the brain's electric fields. Some electrodes are placed on the scalp to record the synchronized activity of the pyramidal neurons, in particular the post synaptic potential (PSP) of these cells [23]. The signal is a voltage difference [μV] between each electrode and a reference, which can be chosen in different ways. The placement of the electrodes on the scalp can be done in different ways, one example is shown in the figure 1.2.2.

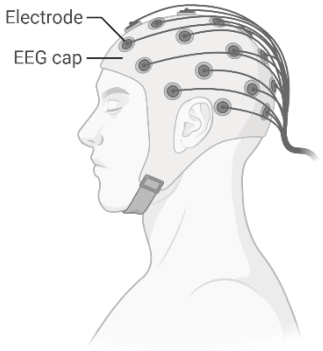

Figura 1.2.2 EEG cap (BioRender)

In this case the electrodes are fixed inside a cap, and a conductive gel is added below each one to reduce impedance and to improve the contact with the skin. The number of electrodes can change as well from 64, 128, 256 but the most used is the first one. The signal is recorded by each electrode, which corresponds to the channel denominated as the 10-20 system.

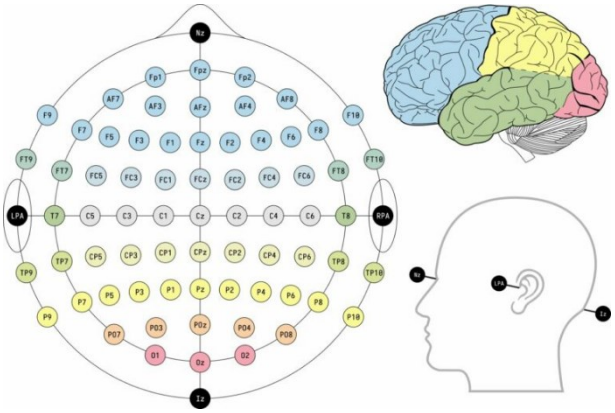

Figura 1.2.3 The 10-20 system with 64 electrodes (BioRender)

One of the main problems faced with EEG concern the distortion of the signal due to the attenuation by the volume conduction through the different tissues. Another important issue is the presence of artifacts, which affects the analysis of the EEG, so for this reason it is essential to remove them from the signal with appropriate methods [24].

The EEG can be divided into two types of registration: the spontaneous EEG and the event related potential (ERP).

The spontaneous EEG refers to the ongoing electrical brain activity recorded at rest, i.e. without external stimuli or tasks. A considerable portion of the signal power originated from the natural rhythmic oscillations in the frequency band between 1 Hz and 40 Hz [23]. This range has been subdivided into smaller functional frequency regions with corresponding names, i.e. delta rhythm (1-4 Hz), theta rhythm (4-8 Hz), alpha rhythm (8-13 Hz), beta rhythm (13-30 Hz) and gamma rhythm (30-200 Hz). The spontaneous EEG is used in epilepsy diagnosis, sleep studies and brain function monitoring.

On the other hand, the ERP**s** are electrical response of the brain to an external stimulus. They are time-locked and phase-locked to the stimulus. They are signal measured in μV and characterized by the shape of the wave, the latency and the amplitude. They can be classified according to the sense organ stimulated, e.g. visual evoked potentials (VEPs), auditory evoked potentials (AEPs) and somatosensory evoked potentials (SSEPs). The ERP are used to asses the functional integrity of specific neural pathways: infact, abnormalities in the latency or amplitude of these waveforms can indicate a dysfunction in that particular pathway.

1.2.3 TEPs

TEPs, transcranial evoked potentials, are a particular type of evoked potential generated by external stimulation via TMS. They represents the measure to study to analyze the propagation of cortical response from the stimulated area to the anatomically connected one [25]. One example is the M1-P15, an early TEP component that occurred after 15 ms from the stimulation of the primary motor cortex, which has been confirmed as a cortical marker for interhemispheric connectivity [26],[27].

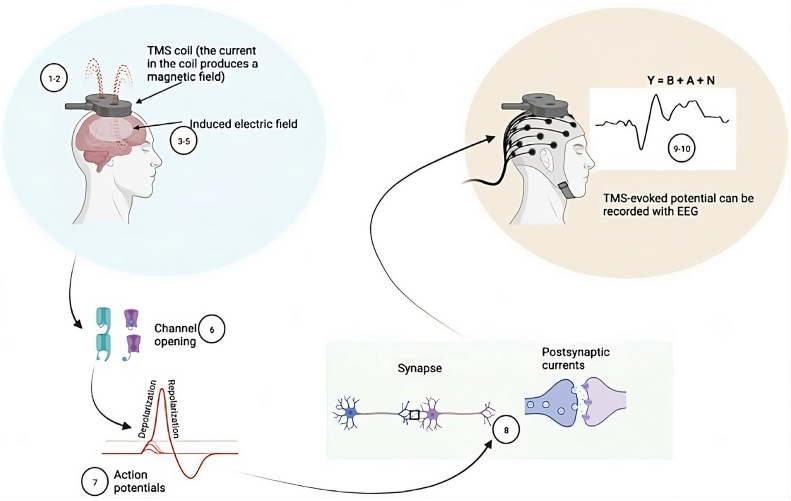

Figure 1.2.4 Schematic representation of the stimulation of TEP [28]

The cascade of events that leads to the generation of a TEP is shown in figure 1.2.4. (1-2) refers to the creation of a magnetic field from the TMS, (3-5) indicates the induction of an electric field in the brain and the production of electric current in the neuronal tissue. (6) indicates the opening of channels (sodium and potassium) and (7) the generation of an action potential. During (8) there is the release of neurotransmitters and the following generation of postsynaptic currents of the pyramidal neurons (9). (10) indicates the potential [μV] recorded from the EEG created by these currents. The signal EEG can be described as a linear model where Y is the EEG recorded signal, B the brain signals of interest, A the sum of the artifacts (e.g., TMS-induced artifacts in the first 5 ms), and N is the noise (e.g., background signal) *[28]*.

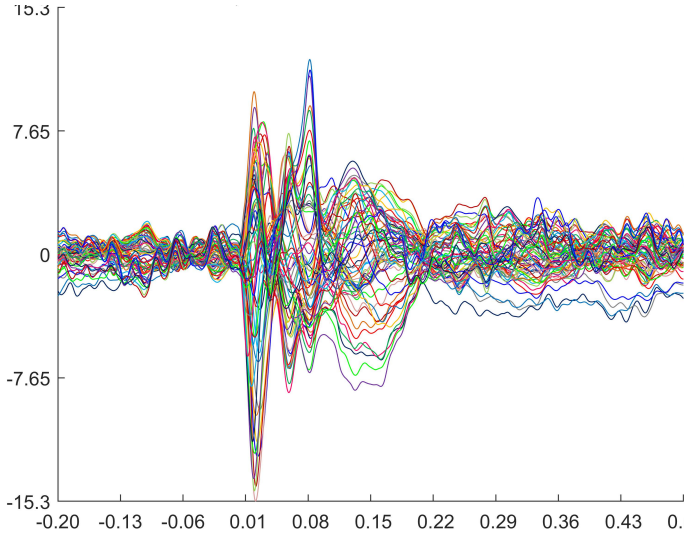

Figure 1.2.5 Visualization of a TEP. Units of measurements: x-axis [s] , y-axis [μV]

A few key points essential for understanding their role in brain research:

- **Real-time modulation**: TEPs are a valuable tool for studying real-time brain modulation due to the high temporal precision of TMS. Infact, the TMS pulse duration is brief (typically 50-100 μs), with stimulation intensities around 1-3 Tesla [28].
- **Variable stimulated area**: the extent of the cortical region stimulated can vary significantly based on several factors, including the geometry of the stimulation coil, the intensity of the stimulus, the specific target area, and the distance between the coil and the cortical surface [29], [30].
- **Non-local effects**: Notably, TMS exerts non-local effects by indirectly activating brain regions that are structurally connected to the primary stimulation site [25], [31]. This characteristic is highly advantageous in brain connectivity research, as TEPs can be observed not only at the stimulated region but also in interconnected areas, including contralateral regions. This supports the concept of TMS's network-level impact, influencing a broader neural network rather than isolated sites alone.

Source reconstruction of TEPs has been shown to be highly reliable, enabling precise tracking of how activity propagates throughout the stimulated network [32]. Research further suggests that structural connectivity significantly influences TEP propagation, i.e. higher density of neural fibers within a network can enhance the spread of signals [33]. This link between structural connectivity and signal propagation underscores the importance of network architecture in understanding how TMS affects brain function [34],[35].

We just cited the concept of source localization, which will be exposed in the next paragraphs, but need to be taken into consideration. Infact, the study of TEPs requires addressing the complex task of EEG source localization, which involves identifying the precise cortical origins of EEG signals recorded during TMS. This passage is challenging due to some intrinsic limitations. The actual approach, which can be considered as the state of the art, consists of performing a source reconstruction on the whole GM and selecting a posteriori the areas structurally connected [33], [34], [35]. For instance, like in our case, assuming we are stimulating a specific point of the M1 cortex (e.g. the hand hotspot), the expected TEP signal can be detected in the connected regions, although with possible variations in latency and amplitude.

Given these considerations, it becomes evident that the study of TEPs has potential applications for the research in demyelinating diseases, such as MS. Infact, the

characteristics of TEPs, such as latency, amplitude, waveform shape, may change in a way to reflect the extent and the location of structural connection damage. By analyzing these variations, researchers can better understand how demyelination affects network communication in the brain, potentially using TEPs as a non-invasive biomarker.

1.4 Source localization

EEG is a long-established method for measuring brain activity and has been widely used in clinical settings, particularly for studying epilepsy, sleep disorders, and dysfunctions of neural pathways. In this context, the term “source localization” refers to the process of determining the specific locations within the brain where neural activity originates, based on signals recorded by methods like EEG and MEG [36]. In the previous chapter, we highlighted how synaptic currents generate electrical flows throughout the head's volume. These flows travel to the scalp surface through a mechanism known as volume conduction [37]. Consequently, the currents create electrical potential differences between the electrodes, which constitute the recorded EEG signals.

Source localization presents significant challenges in neuroscience due to various factors. The primary difficulty arises from the non-linear propagation of electrical signals through the complex structures of the brain and skull, which distort the recorded signals. Additionally, the EEG suffers of poor spatial resolution that makes it difficult to infer the location of the brain areas generating the neuronal activity measured on the scalp [38]. Furthermore, the simultaneous activation of multiple brain regions complicates the analysis even more, as it adds to the ambiguity in determining the precise locations. For these reasons, this problem needs to be faced employing computational algorithms and detailed models to create more reliable reconstruction of the neuronal activity.

The EEG source reconstruction requires a complex pipeline that can be divided into the forward and the inverse problems which are presented in the following paragraphs.

1.4.1 Forward problem

The term “forward problem” refers to the process of determining the potential at each scalp electrode generated by a known source in the brain [39]. It requires creating a model to simulate the propagation of neural currents generated by specific brain regions throughout

various tissues in the brain. Before going into the details of the model, it is important to an give an overview of the mathematical equations that underlie the process.

Many signal processing techniques can be modelled as linear systems, where the output for a combination of inputs is simply the sum of the outputs for each input, in accordance with the superposition principle [40]. This principle applies to EEG signals and is particularly relevant for linear source estimation methods, like the L2-minimum norm estimate. Infact, if two brain sources are active simultaneously, the resulting spatial distribution of the signals at the electrodes will be the sum of the individual spatial distributions of each source.

This linearity simplifies the process of source estimation, but in real-world scenarios, there is typically simultaneous activity of multiple sources in the brain, which adds complexity. Estimating the locations and strengths of multiple active sources at once is more challenging than dealing with a single source, but the superposition principle can still be exploited in reconstruction algorithms to address this complexity effectively. The figure 1.4.1 illustrates the principle just exposed.

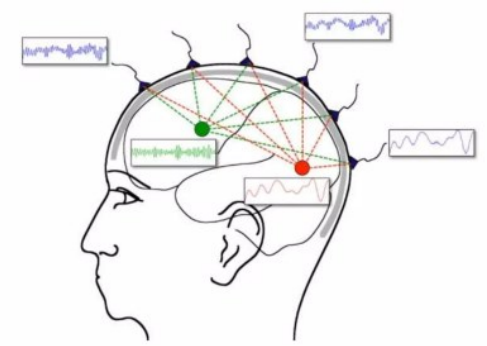

Figure 1.4.1: Superposition principle applied to EEG signal

Mathematically, we can write down the following equation:

$$d = Ls + e \qquad (1)$$

where $d(mx1, m:\text{number of channels})$ represents the data in m channels, so the EEG signal, s ($n\,x\,1$, n: number of neural sources), L ($m\,x\,n$), the so-called leadfield matrix which contains information about head geometry (shape and conductivities), measurement configuration (sensor types and position), and the physics of signal generation (quasi-static approximation of Maxwell's equation) [41], and e ($m\,x\,1$) is the noise term [40].

After the brief presentation of the mathematical theory, the next paragraph is going to summarize the steps to be conducted to compute a forward model. First of all, it is necessary

to specify that if the purpose is to make an individualized source reconstruction, it is highly recommended to use the structural MRI image to extract the individual information. Otherwise, it is possible to use a template brain.

The figure 1.4.2 illustrates the pipeline employed for source reconstruction, following the instructions of the open-source software FieldTrip. Brain activity can be estimated from the EEG signals measured on the scalp, along with anatomical and spatial information. The sensor configuration is essential for determining the spatial arrangement of the electrodes, as well as the geometrical and conductive properties of the head, which are essential features of the head model. Additionally, the location of the sources is represented in the so-called source model. The anatomical and spatial information is used to calculate the lead field, which establishes the relationship between the electrical activity at a specific electrode and the activity of various sources within the brain. The accuracy and anatomical fidelity are essential to ensure reliable source localization [42]. More details regarding each steps have been explained in the following chapters.

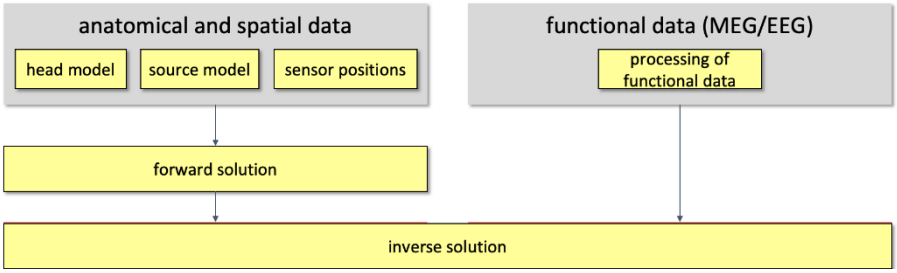

Figure 1.4.2: Overall outline of the pipeline used for source reconstruction

1.4.2 Inverse problem

The term "inverse problem" refers to the estimation of the unknown sources corresponding to the measured EEG signal. This represents a significant challenge because of the ill-posed nature of the problem, i.e. small changes in the data can results in large differences in the estimated sources, and the non-uniqueness problem, as there can be different solutions that generate the same potential field registered on the scalp. Due to the last issue, a priori assumptions need to be incorporated, e.g. purely mathematical, anatomical or biophysical constrains [43].

Mathematically, according to the Eq. *(1),* the Eq. *(2)* can be written as follow:

$$s\_est = Kd = K(Ls + e) = KLs + Ke = Rs + Ke \quad (2)$$

where s_est represents the estimate for source distribution, K $(n \times m)$ can be seen as a linear matrix, R $(n \times n)$ the resolution matrix, provides the desired relationship between true and estimated sources, except for the last term that reflects how noise is transformed from signal space into source space [40].

There are various approaches to perform source reconstruction, but they fall into two main categories: dipole source localization and distributed source localization.

The dipole source localization technique assumes that brain activity originates from a small number of focal sources, modelled as dipoles. This approach is based on the equivalent current dipole (ECD) model, which represents each source region with a dipole that is characterized by location, orientation, and strength. Pyramidal neurons generates dipoles with opposing charges. In this model there are different approaches, such as fixing the location and/or the orientations [44]. This technique is most effective when certain conditions are met:

1. The number of unknown parameters is smaller than the number of EEG sensors,
2. The source activity can be accurately modelled by a few dipoles,
3. The number of dipoles is predefined.

These conditions help ensure that the model has enough constraints to solve the inverse problem with reasonable accuracy.

Dipole fitting typically involves optimization techniques to minimize the difference between the observed EEG data and the potentials predicted by the model. Despite its limitations, such as being less suitable for distributed brain activity, this method continues to be used in clinical applications, particularly for localizing epileptic foci.

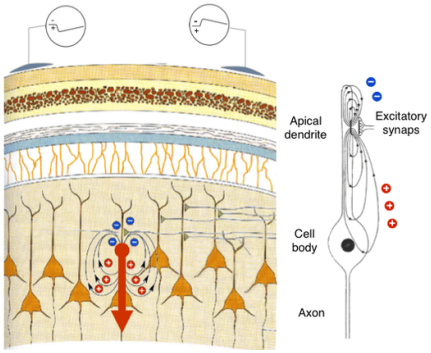

Figure 1.4.3: Schematic representation of ECD

The alternative approach is the distributed one, specifically the distributed source localization methods, which do not require a priori assumptions regarding the number of dipoles. In this framework, the reconstruction of the signal is performed at each point within a source grid that typically covers the entirety of the GM, although anatomical constraints may be incorporated. Consequently, the distributed model is used when activity is not expected to be limited to a few specific sources, but rather is spread over various regions of the brain.

The most widely used distributed source models are variations of a solution originally proposed by Hämäläinen and Ilmoniemi [45], known as the minimum norm solution (MN). This solution is based on the minimization of the total energy of the current distribution over all solution points (minimizing the least-square error, i.e. the L2-norm) [46]. The Eq. (3) give the solution for the resolution matrix:

$$R_{MNE} = L^T (LL^T + \lambda C)^{-1} L \qquad (3)$$

where λ is the regularization parameter and C *(m x m)* the noise covariance matrix.

Minimizing the effect of noise, specifically the term Ke in Eq. (2), is crucial for improving the accuracy of source estimation. This is typically achieved through Tikhonov regularization: it introduces a trade-off between spatial resolution and sensitivity to noise [47]. The degree of regularization in source reconstruction is determined by the regularization parameter, commonly represented as λ (lambda). In particular, higher values of λ results in lower spatial resolution and reduced goodness of fit, leading to a significant loss of detail and variability in the reconstructed activity. Inversely, an increased smoothness on source estimates is observed [48]. While the specifics of the regularization procedures are not the primary focus of this thesis, it is important to highlight that various methods exist for selecting the optimal value for this parameter, such as the Generalized cross-validation [49] or L-curve [50]. However, it is important to determine an opportune value for λ, which can be determined with computational tools that derive this value form the assumed signal to noise ratio (SNR) of the data [40].

However, this MNE approach has a significant limitation: it tends to be biased toward superficial sources due to their spatial vicinity to the sensors. For this reason, other methods have been implemented to overcome this limitation, e.g. the so-called weighted minimum norm (WMN) solutions. In this case, the equation is the following:

$$K_{wMNE} = DL^T \left(LDL^T + \lambda C \right)^{-1} \quad (4)$$

where D is the diagonal weighting matrix chosen to increase the impact of deep sources, e.g., based on the vector norms of the leadfield columns (topographies of deeper sources tend to have smaller norms). A variation of WMN is the low resolution electromagnetic tomography LORETA [51] in which the norm of the second-order spatial derivative of the current source distribution is minimized to ensure spatial coherence and smoothness. There exists others techniques based on MNE, e.g. variations of LORETA (e/s LORETA), dSPM [52], and LAURA (Local AUtoRegressive Average) [53].

Consequently, different academic and commercial software packages have been developed. Such advancements have significantly improved the accessibility and usability of EEG source localization methods, allowing a broader range of users, from neuroscientists to clinicians, to apply these techniques in their work.

Name	Website	Inverse models
ACADEMIC SOFTWARE PACKAGES		
Brainstorm	https://neuroimage.usc.edu/brainstorm	Dipole modeling, Beamformer, sLORETA, dSPM
Cartool	https://sites.google.com/site/cartoolcommunity/	Minimum Norm, LORETA, LAURA, Epifocus
EEGLab	https://sccn.ucsd.edu/eeglab/index.php	Dipole modeling
Fieldtrip	http://www.fieldtriptoolbox.org/	Dipole modeling, Beamformer, Minimum Norm
LORETA	http://www.uzh.ch/keyinst/loreta.htm	LORETA, sLORETA, eLORETA
MNE	https://martinos.org/mne/stable/index.html	MNE, dSPM, sLORETA, eLORETA
NUTMEG	https://www.nitrc.org/projects/nutmeg	Beamformer
SPM	https://www.fil.ion.ucl.ac.uk/spm/	dSMP
COMMERCIAL SOFTWARE PACKAGES		
BESA	http://www.besa.de/products/besa-research/besa-research-overview/	Dipole modeling, RAP-MUSIC, LORETA, sLORETA, LAURA, SSLOFO
brainvision analyzer	https://www.brainproducts.com/	LORETA
BrainVoyager	https://www.brainvoyager.com/	Beamformer, Minimum Norm, LORETA, LAURA
GeoSource	https://www.usa.philips.com/healthcare/solutions/neuro/neuro-research-applications	Minimum Norm, LORETA, sLORETA, LAURA
CURRY	https://compumedicsneuroscan.com/curry-source-reconstruction/	Dipole modeling, MUSIC, Beamformer, Minimum norm, sLORETA, eLORETA, SWARM

Figure 1.4.4: Non-exhaustive list of academic and commercial software packages for EEG source localization (Hauk et al., 2022).

1.5 Thesis objectives

The research presented in this thesis was conducted during my internship at Neurophysiology Lab, IRCCS Centro San Giovanni di Dio Fatebenefratelli in Brescia, Italy. The key objective of the study was the implementation of a new source reconstruction method of TEPs. This new approach aims to incorporate a priori information about the specific locations of the source models within the GM, limiting the reconstruction to these targeted regions, i.e. those structurally connected to M1 cortex. These regions can be individually estimated for each subject using tractography, thus preserving inter-subject

variability. However, due to technical issues, it was not possible to utilize this information in the present study. Nevertheless, the work by Nozais et al., 2023 [9] provided access to a detailed resting-state atlas of motor domains. Finally, the proposed method has to be compared to the existing state-of-the-art approaches to evaluate its performance and efficacy.

The pilot study aims to refine existing source localization techniques in healthy individuals, with the hope to extend its application in pathologies characterized by structural damages of the interneurons connections, e.g. MS pathology. Brain connectivity plays an important role in this work, as the interaction between GM regions and their structural connections via WM pathways is essential for understanding how structural disruptions may impact neural activity. The hope is to contribute to the development of pragmatic tools that could potentially identifying biomarkers for pathological conditions.

2. Materials

This chapter contains the presentation and the description of the dataset that has been used in the implementation of the methods and in the following analysis.

2.1 TEPs

The dataset is described in the work of Bortoletto et al., 2021 [26] and the data collection was supported by Italian Multiple Sclerosis Foundation (FISM). For completeness, the relevant portion of the data will be transcribed here, even though it is already presented in the paper.

The sample was composed by twenty healthy partecipants, with mean age: 34 years (range 26-47 years), of whom 9 females. Single biphasic TMS pulses were delivered with a C-B60 coil (MagPro X100 including MagOption, MagVenture) over the left and right hemispheres. The M1 hotspot was functionally identified as the location that consistently elicited motor evoked potentials (MEPs) in the abductor pollicis brevis (APB). Neuronavigation assistance was provided by the SofTaxic system (EMS, Italy), which allowed for coregistration of the T1 anatomical MRI with the head position during stimulation.

A TMS-compatible system (BrainAmp, Brain Products GmbH, Munich, Germany) was used to record EEG data from 67 channels, with the nose as the reference and FPz as the ground. In addition, vertical and horizontal electrooculogram (EOG) and electromyography (EMG) from the abductor pollicis brevis (APB) were added. The amplifiers were set to a sampling rate of 5 kHz, with an online bandpass filter ranging from 0.1 to 1000 Hz. Impedance was kept below 5 kΩ, allowing for the capture of TMS artifacts with a duration as brief as 5 ms. [54].

The specific details of the experimental setting are not essential to report in this thesis, as not of interest. What is important to note is that the TEP data analyzed in this study was the ones obtained from the stimulation of the left M1 cortex during a no-task condition.

The preprocessing steps that has already been completed by the researchers are listed in the next lines. This analysis was performed in MATLAB with custom scripts using EEGLAB [55] and FieldTrip [56]. Two other methods were used: source-estimate-utilizing noise-discarding (SOUND) algorithm [57] and the signal-space projection and source-informed reconstruction (SSP-SIR) algorithm [58]. Then the EEG was interpolated around the TMS pulse (from -1 ms to 6 ms), high-pass filtered (0.1 Hz), epoched (from -200 ms to 500 ms) and downsampled to 2048 Hz. With the use of SOUND, measurement noise was discarded

(spherical 3-layer model, regularization parameter: $\lambda = 0.01$). The following steps were carried out: visual inspection, artifact rejection, and independent component analysis (ICA) to correct for ocular artifacts. TMS-evoked muscular artifacts occurring within the first 50 ms were removed using SSP-SIR (0–3 muscle artifact components per dataset). The data were then low-pass filtered at 70 Hz and re-referenced to the average of TP9 and TP10. Finally, following a second round of visual inspection and artifact rejection, the TMS-EEG data were baseline-corrected from -100 ms to -2 ms before the TMS pulse and then averaged.

The preprocessed data obtained from this pipeline served as the starting point for my analysis, upon which I implemented additional steps to achieve my research objectives. Specifically, I excluded electrodes 66-69 (EOG and EMG channels), I calculated the covariance matrix, and then re-referenced to the average.

2.2 Structural MRI

These data of the twenty-one healthy subjects are described in [26]. T1-weighted, T2-weighted and DTI were acquired, but for our purpose only T1-weighted was considered. Infact, high-resolution T1-weighted 3D anatomical sequences (TR = 2400 ms, TE = 2 ms, size of voxel = 0.9 mm, isotropic resolution) were acquired.

2.3 WhiteRest atlas

Our initial goal was to identify the GM regions structurally connected to the left M1 TMS stimulation point. The original plan involved generating individual tractography for each participant and using this to create GM maps of interest. However, the findings reported in Nozais et al., 2023 [9] have proven to be highly relevant and interesting for our work. Infact, in this paper, Whiterest atlas is presented: it is composed by 30 resting-state networks (RSNs), and it has been created by combining functional MRI (fMRI) and tractography to map the brain's connectivity in a more integrated and comprehensive way. The fMRI, which measures brain activity by detecting changes in blood oxygenation levels (BOLD signal), was used to identify functional GM regions, while tractography was employed to map the structural connections formed by WM tracts. These WM pathways are responsible for communication between distant brain regions. The Whiterest atlas therefore offers a

powerful tool for studying how GM regions are not only locally active but also how they interact with each another through long-range WM connections. This integrated view is critical for advancing research in neuroscience, expecially in pathological condictions where disruptions in either structural connectivity or functional activity can have significant effects on brain functionality.

For this project, we specifically focused on the GM map of RSN 08, which is associated with the right hand motor network. The z-map in MNI (Montreal Neurological Institute) coordinates was downloaded from Neurovault.org, then thresholded ($z > 7$), and a binary version was created for the next analysis.

3.Methods

This section represents the core of the thesis, as it shows the steps implemented to achieve our goal.

The chapter is structured into two main sections: the first section addresses the solution to the forward problem, while the second section focuses on the inverse problem, describing the implementation of two distinct methods.

Each step in this section has been implemented using the software MATLAB R2024a, the toolbox software Fieldtrip [56] and SPM12 toolbox. Here are reported the main steps of the procedure.

3.1 Solving EEG forward problem

The following pipeline for the forward computation was applied to each of the twenty subjects described in the chapter 2. The figures and the data presented in this sections are the one obtained by the subject number 2 (SC_02).

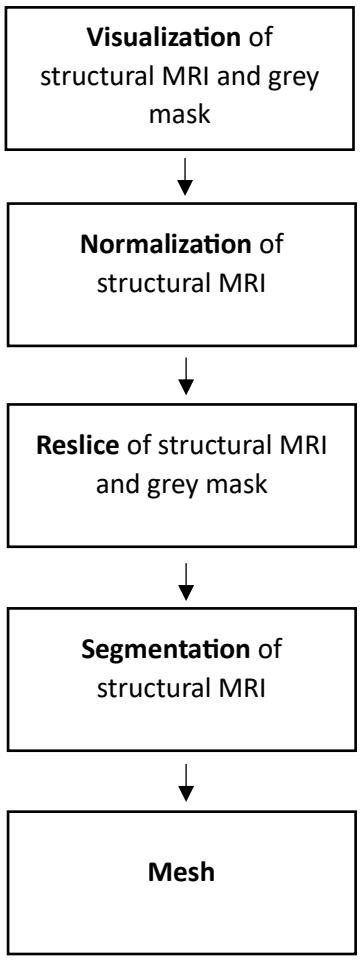

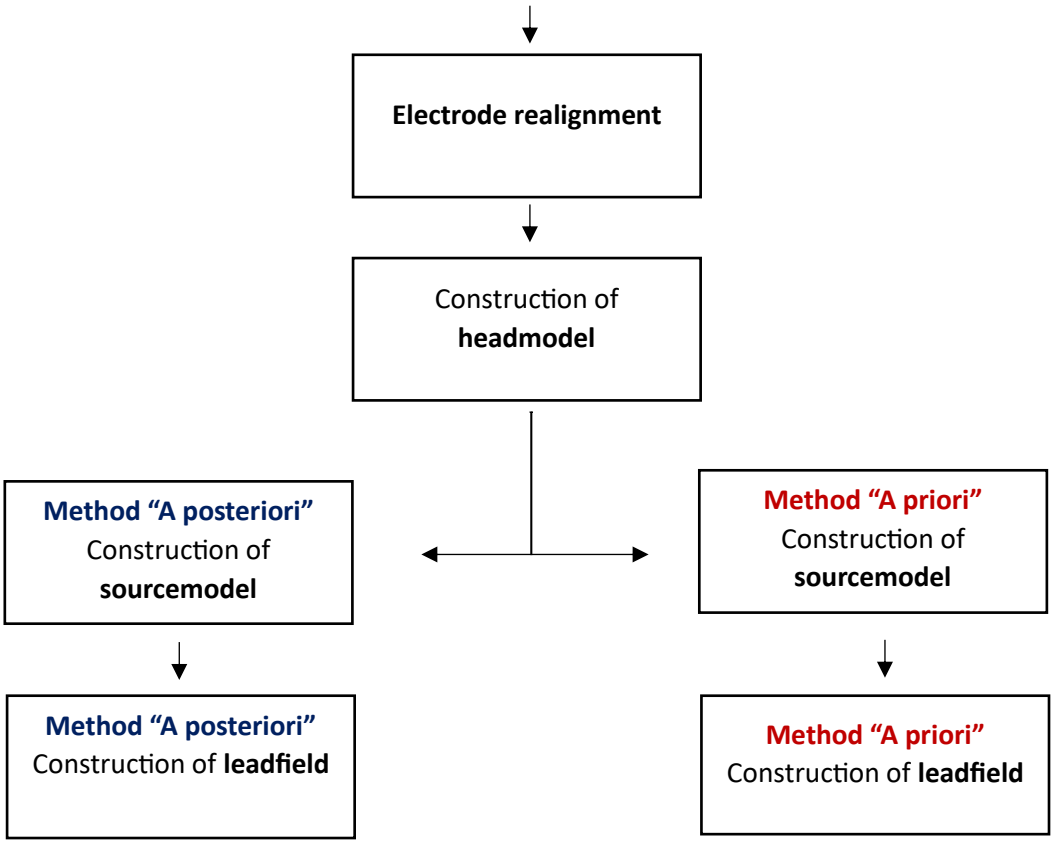

Figure 3.1.1: pipeline for forward model

This section consists of several steps, which will be outlined in detail through the following bullet points.

1. **Visualization of structural MRI**: loading and reading of the anatomical data, i.e. the structural MRI, expressed in native coordinates.

   The functions used in this section are **ft_read_mri** and **ft_sourceplot**. In Figure 3.1.2, the **ft_sourceplot** function allows visualization of the MRI in three anatomical views: sagittal, coronal, and axial. Additionally, it provides references to voxel numbers, indices, and locations within the coordinate system. It is possible to navigate through the figure, enabling the visualization of the MRI slices in a dynamic way.

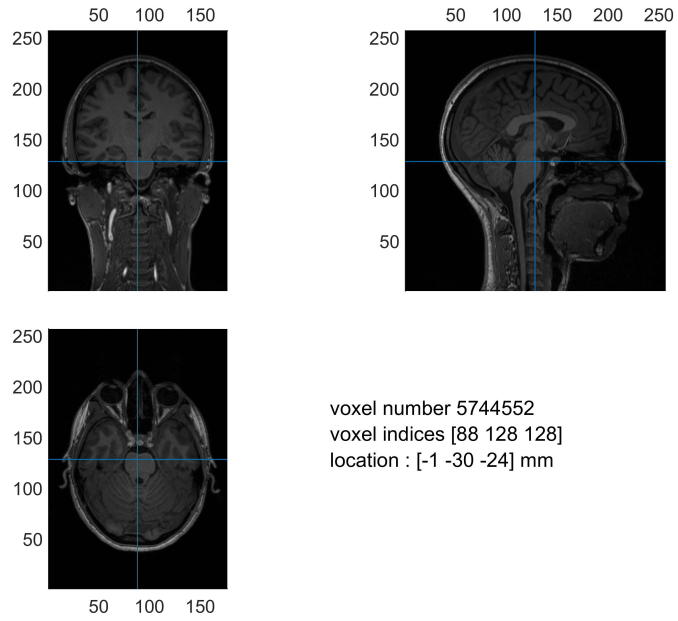

Figure 3.1.2: visualization of the individual MRI

2. **Visualization of the grey mask (RSN_08):** loading and reading of the binary version of the RSN_08 (MNI coordinates) from the WhiteRest Atlas. As mentioned in the chapter 2, the z-map of the RSN_08 was threshold at |z| > 7, considering only the most significant (and involved) areas [9]. A binary version of it is represented here:

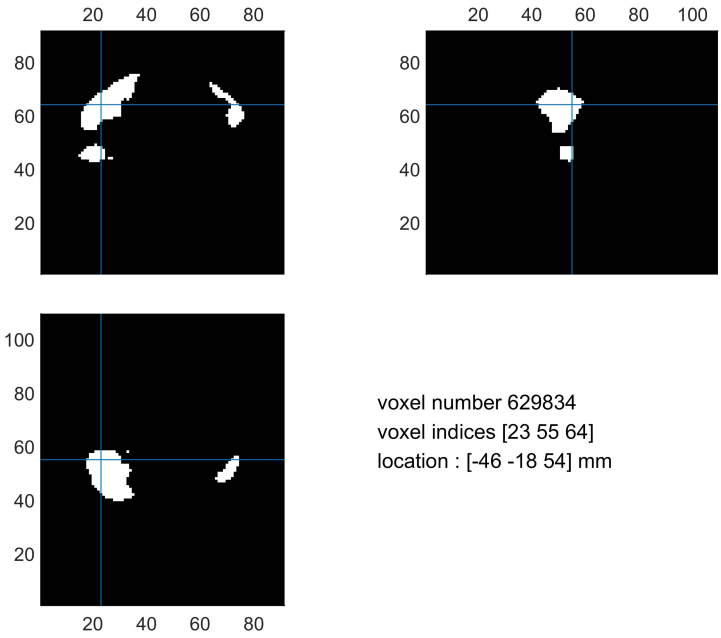

Figure 3.1.3: visualization of the grey mask

3. **Normalization of the structural MRI:** normalization (**ft_volumenormalize**) of the individual MRI to the MNI coordinates (like the grey mask), after using the function **ft_determine_coordsys** to add the coordinate information in the structure file of the image.

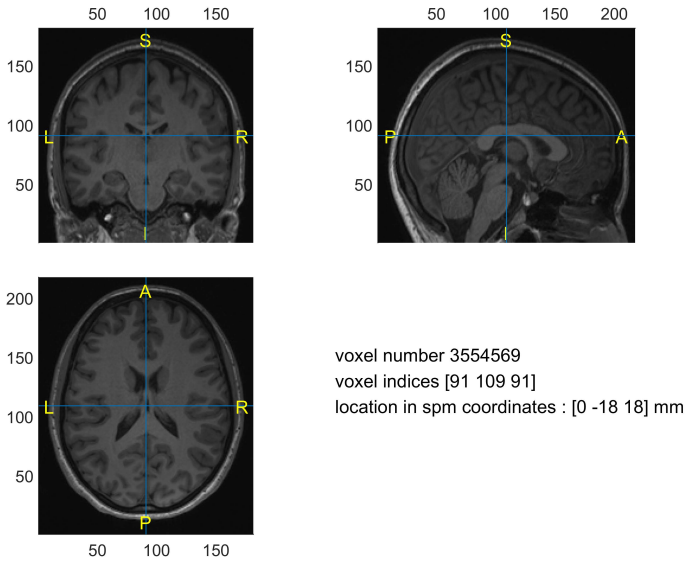

Figure 3.1.4: visualization of the mri normalized

4. **Reslice of structural MRI and grey mask:** reslicing (**ft_volumereslice**) of the two images, i.e. in both dimensions and voxel size are the same (256 each direction, 1 mm x 1mm x 1mm). Now the structural MRI is correctly aligned to the GM, which can be considered as our template, it is possible to continue with the next image processing steps. The figure obtained form the reslicing of the GM is not shown as not relevant to visualize.

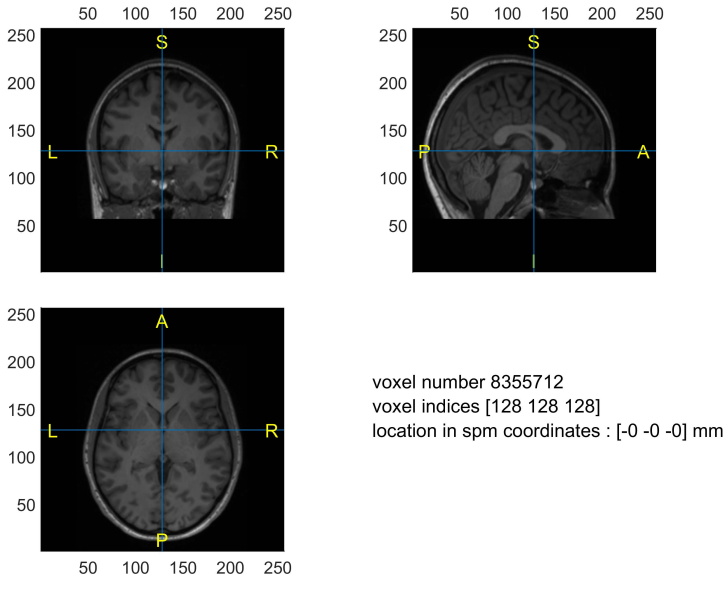

Figure 3.1.5: visualization of the mri resliced

5. **Segmentation of the structural MRI:** segmentation of structural MRI (**ft_volumesegment**). The segmentation is the process of dividing the image into different regions (segmentation) corresponding to specific tissues. In this case the choice has been to implement a FEM (Finite Element Method) which gives the opportunity to distinguish between GM (orange in the figure 3.1.5), WM (white), CSF (dark orange), skull (green) and scalp (purple).

   There are several approaches to incorporating realistic head geometries in EEG source reconstruction. The three most used methods are the standard spherical model [59], the boundary element method (BEM) [60],[61] and the finite element method (FEM) [62]. In addition, alternative techniques such as the finite volume method (FVM) [63] and the finite difference method (FDM) [64] exist, but they were not considered in this study. Specifically, the FEM model was chosen due to its demonstrated ability to enhance source localization accuracy and provide more reliable EEG source reconstructions [65],[66]. The segmentation details follow the default settings implemented in the corresponding FieldTrip function.

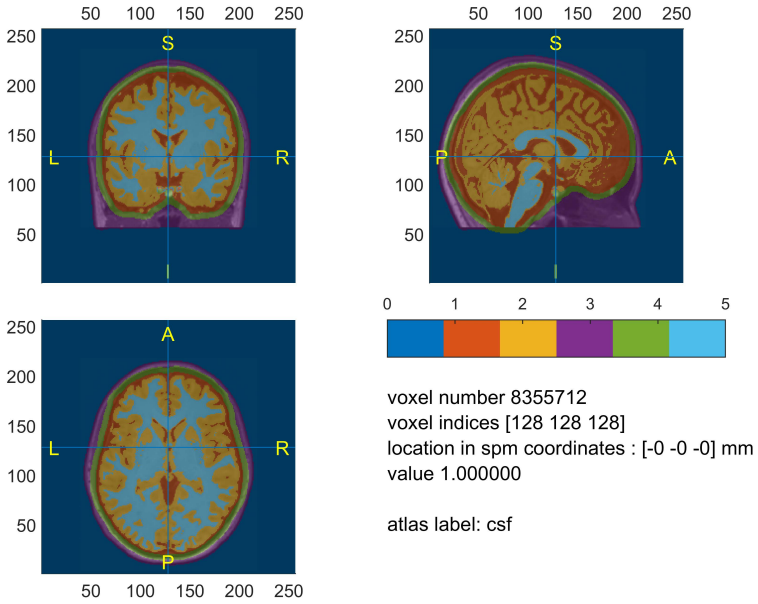

Figure 3.1.6: visualization of the segmentation

6. **Mesh:** creation of the mesh **(ft_create_mesh).** The mesh is a geometric representation of a complex object, e.g. the head, which is composed of smaller, connected elements. In this case, the input consists of the segmentation from the

previous point and the elements are hexahedral, following the approach outlined in the work of Vorwerk et al. [65].

7. **Electrode realignement**: realignment of the electrode structure to the head model (**ft_electroderealign)**. This allows for the manual alignment of the electrode coordinate system to the head model by specifying key anatomical landmarks: nasion, inion, right auricular, and left auricular points.

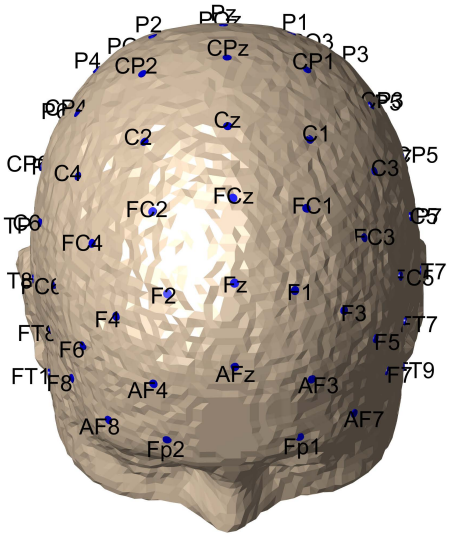

Figure 3.1.7: visualization of the scalp and the electrodes

8. **Headmodel:** creation of the headmodel **(ft_prepare_headmodel).** In this section, it is necessary to specify the electrical conductivities $[\frac{S}{m}]$ of the different tissues to accurately calculate the stiffness matrix. These conductivity values are consistent with those used by FieldTrip, based on the work of Vorwerk et al. [37] and available literature [67].
   The stiffness matrix is a mathematical construct commonly used in finite element analysis which in this context represents the relationships between nodes in a mesh, describing how electric currents propagate through different tissues.

9. **Sourcemodels:** The implementation of the two source models is described here **(ft_prepare_sourcemodel),** following the approach recommended by FieldTrip, as cited earlier in [65]. The method constructs a grid of source points $[mm]$on the GM

based on the chosen resolution (6 mm) and the provided head model. It aligns these grid points with the centroids of the hexahedral elements in the mesh, ensuring anatomical precision. Each grid point can then serve as a potential source location for neuroimaging analyses.

The choice of a 6 mm resolution was determined through multiple trials to ensure the second source model provides a comprehensive grid that sufficiently covers all relevant locations within the RSN_08 GM.

Infact, it was necessary to generate two distinct source models: the first covers the entire GM, while the second focuses specifically on grid points that lie at the intersection between the full source grid and the GM maps of the RSN_08. The figures 3.1.8, 3.1.9, 3.1.10 show the source grid points across the whole GM, highlighted in yellow. The regions derived from the WhiteRest atlas are shown in gray (ROIs, regions of interest).

The figures 3.1.11, 3.1.12, 3.1.13 show the regions from the previous figure, with the source grid points inside the seven ROIs, represented in different colours.

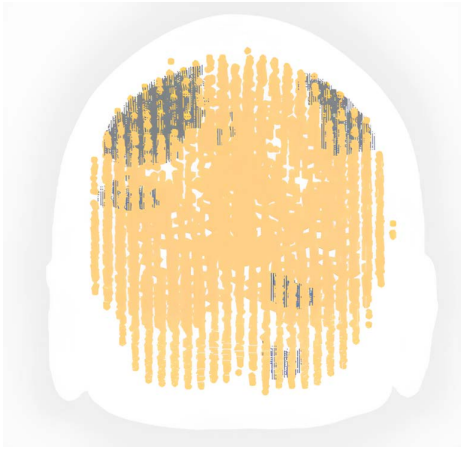

Figure 3.1.8: visualization of the source grid (yellow) covering the whole GM (coronal view)

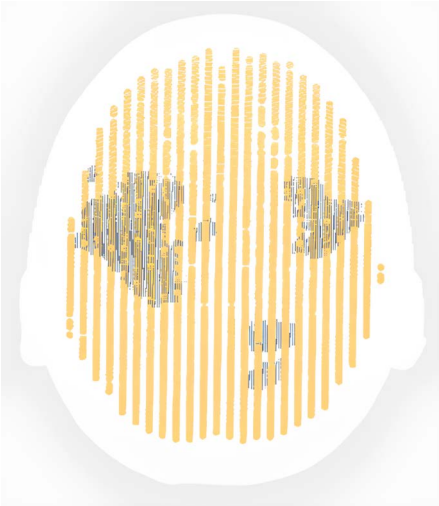

Figure 3.1.9: visualization of the source grid (yellow) covering the whole GM(axial view)

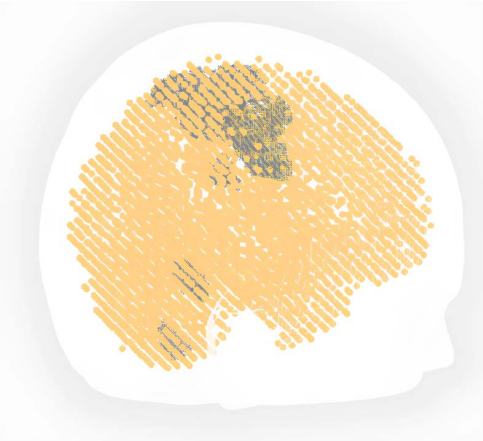

Figure 3.1.10: visualization of the source grid (yellow) covering the whole GM(sagittal view)

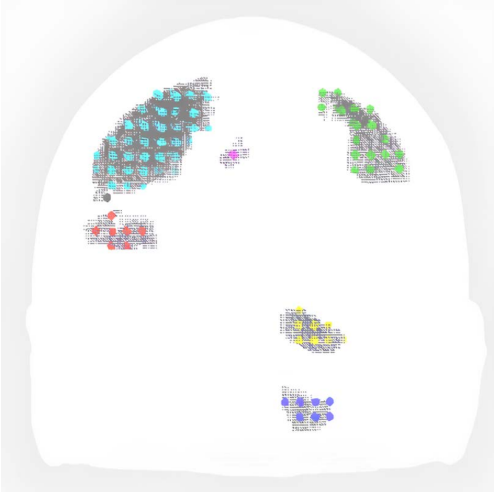

Figure 3.1.11: visualization of the source grid (different colours) inside the ROIs (coronal view)

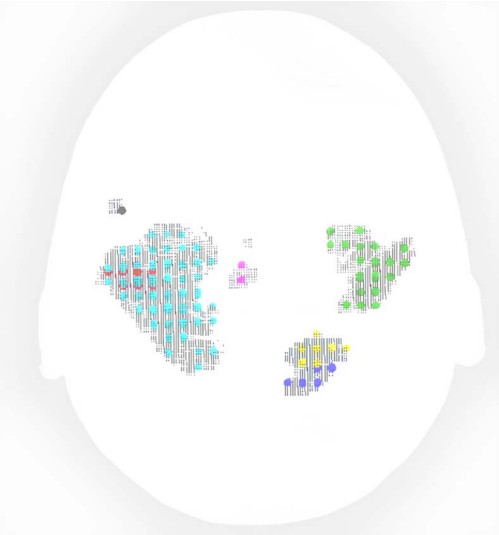

Figure 3.1.12: visualization of the source grid (different colours) inside the ROIs (axial view)

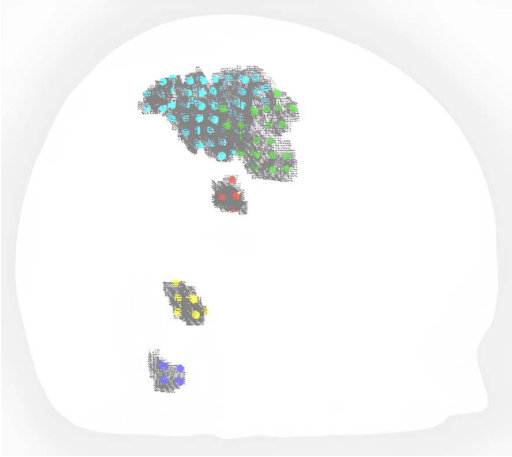

Figure 3.1.13: visualization of the source grid (different colours) inside the ROIs (sagittal view)

In this research, I chose to incorporate a priori information in the following way:

- **Binarization of the fMRI-DTI mask**: application of a threshold ($z > 7$) to the fMRI-DTI mask, transforming it into a binary format.
- **Sourcemodel creation**: binarized map was used to construct the sourcemodel.

This approach is similar to previous methods used by others [78], with a key difference: here, the constraints combine functional information from fMRI with

structural information from DTI. This integration addresses one significant limitation of fMRI-EEG studies, namely, the discrepancy in temporal resolution between fMRI and EEG data.

Although other techniques could potentially be applied to optimize the fMRI-based priors, these were not explored in this study [68], [52], [69]. However, they represent an interesting direction for future research and could further enhance the integration of structural-functional data.

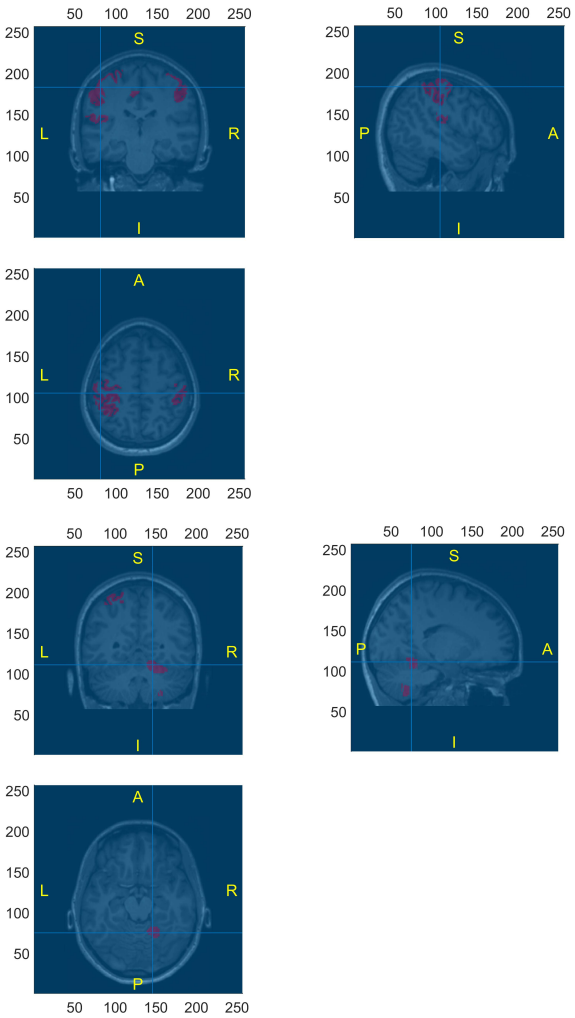

Figure 3.1.14: visualization of the areas of interest (purple) from two different points

From the figure 3.1.23 it is possible to better visualize the anatomical location of the interested grey areas (purple). The areas that has been found are relative to what inside the WhiteRest Atlas is described as a portion of the motor network, and it includes different areas with variables extension. The study focuses on five ROIs consistently observed across all subjects. The regions marked in black and magenta,

located near the left primary motor cortex and part of the precentral gyrus, were not included in the analysis due to their absence in two subjects. The other ROIs that has been individualized correspond to the stimulated area on the left hemisphere (cyan), which includes the left precentral gyrus and the left postcentral one, then the contralateral area on the right (green), two regions in the right part of the cerebellum (yellow and blue) and another area under the stimulated area and linked to this one (red). These ROIs were localized using the MRIcron software, which aided in verifying and naming each region through alignment with both the fMRI-DTI atlas and the structural MRI scans of each subject. In conclusion, seven distinct ROIs were identified, representing components of the sensorimotor network in the left hemisphere, associated with the right hand.

Consequently, two distinct source models were created: a larger one covering the entire GM and a restricted model focusing on the seven ROIs. It is important to emphasize that both source models were tailored for each individual subject due to the incorporation of their individual MRIs. This individualized approach enables a more accurate analysis of neural activity, taking into account the inter-individual variability.

10. **Leadfield:** computation of the leadfield **(ft_compute_leadfield).**

    It computes the forward solution for a dipole in a volume conductor model. It is expressed as the leadfield matrix $[\frac{V}{A\,m}]$ and it requires, as input, the headmodel, the sourcemodel and the electrode configuration. The leadfield in MATLAB is organized as a cell array, each corresponding to a position in the source model within the brain. Each of these cells contains an $N_{channels}\ x\ 3$ matrix, where $N_{channels}$ is the number of EEG channels (65), and 3 represents the three axes of orientations (x,y,z). This matrix represents the field distribution across all channels for a dipole source located at that specific position. So, the entire cell array includes all possible source locations defined in the source model. In our case, we compute two different leadfields because of the two different sourcemodels.

3.2 Solving EEG inverse problem

At this stage, after the resolution of the forward model and the loading of TEPs data, it is possible to discuss the source reconstruction phase.

3.2.1 Method “a posteriori”

The word “a posteriori” refers to the method considered the state of the art [34].

For this part it has been implemented the MNE source reconstruction using the function **ft_sourceanalysis.** The function was configured with specific parameters, following the default settings recommended by FieldTrip according to [52], [70],[71].

- **Method**: MNE (Minimum norm estimate);
- **Latency**: the entire duration of the TEP (from -0.2 s to 0.5 s, 1434 samples);
- **Grid**: the leadfield grid, calculated across the whole GM;
- **Headmodel**: calculated in the analysis;
- **Prewhitening**: applied to the data (set to "yes");
- **Lambda value**: set to 3;
- **Source covariance matrix scaling**: applied to the data (set to "yes").

In particular, it is necessary to give other details:

- **Noise covariance** ($N_{channels}\ x\ N_{channels}$): it represents the noise covariance across the channels, and it has been calculated from the TEP data;
- **Noise lambda**: not applied to the data (default setting equal to 0);
- **Source covariance** ($N_{source}\ x\ N_{source}$): it represents the source covariance, allowing for specific assumptions about the source activity spatial distribution. Not specified (default setting is an identity matrix), assuming all the sources are independent;
- **Labda:** scalar value for the regularizarion**.** It could be estimated from the SNR of the data, but in the case of TEP it is very difficult to estimate this measure as the presence of a certain amount of noise not negligible which can remain after the preprocessing phase. However some trials has been done varying the lambda value, but the ultimate decision was to keep fixed this term to the value 3.
- **Prewhitening:** it is a process on the leadfield matrix by accounting for noise variance. Specifically, it involves using a noise covariance matrix to condition the leadfield data, which can improve source estimation accuracy by reducing the impact of noise on the solution. When this setting is applied, the signals across channels are decorrelated and normalized, which helps avoid potential numerical issues.

- **Scaling of the source covariance matrix:** this setting adjusts the source covariance matrix so that the average of the source signals is normalized relative to the measurement noise. This is another important adjustment to improve the source localization solution.

The **ft_sourceanalysis** function provides a structured output, which contains the following fields:

1. **Coordinates (coordsys)**: the coordinate system (spm);
2. **Unit (unit)**: the unit of measurement (m);
3. **Time (time)**: the entire latency we selected in the previous options;
4. **Position (pos)**: the 3D coordinates of each source point in the brain volume;
5. **Gray matter indicator (inside)**: a logical vector that marks positions within the GM of the brain, with a value of 1 for valid positions of the source model.
6. **Source amplitude and power (avg)**: represents the intensity of neural activity over time at each source location, as well as relevant noise covariance information. Specifically, within this field, the dipole moment (**mom**) is included ($Nsources$ cells). Each entry in this cells corresponds to the dipole moment at each source location over time, reflecting the strength and orientation of the estimated neural activity.

Finally, it was important to select the solutions corresponding to specific areas of interest while also considering those outside these regions. This "a posteriori" selection process is what characterized the model described in this section.

3.2.2 Method "a priori"

According to the first ideation of this project, using a dipole fitting model approach (ECD) would have been optimal due to the limited number of sources representing the areas of interest we expected. However, this method proved inadequate in this case because of the spatial extension and the number of these areas. Consequently, it was decided to adopt the same model as the "a posteriori" method focusing on how to implement the "a priori" information effectively.

As already said in the section 3.1, the creation of the second sourcemodel gives the opportunity to select the location desired, i.e. the M1 connected regions. The

implementation of this method was largely consistent with the earlier approach; however, the key difference is in the source model itself. In this case, the source reconstruction was restricted to the grid points representing these targeted areas.

In Section 3.1, a description and a corresponding figure illustrate the two distinct source models, providing a clearer understanding of the concepts presented.

4. Results

The statistical analysis has been conducted on both the methods: initially, the method "a posteriori" has been analysed to verify its proper implementation. After this, a second analysis was performed on the other method, examining:

- The **main effect of the method**, assessing the impact of the chosen method on the outcome variable;
- The **main effect of the ROIs**, focusing on the effect contributed by each individual ROI;
- The **ROI-method interaction**, to explore how the impact of the method varies across different ROIs.

The analysis focuses on the activation signal, specifically the amplitude of the electric dipoles [$A\,m$] identified for each point of the source model. The time interval was set between 0.005 and 0.35 seconds [0.005-0.35 s] to avoid the TMS pulse artifact, which lasts up to 5 ms [54], and to focus on the early-middle response. The correction for multiple comparison has been necessary for the control of the multiple comparison problem, typical when dealing with EEG signal analysis.

A further step that was performed was a quality check on the outcomes of each subject, comparing the results of topographic activation maps obtained with the sLORETA software.

4.1 Verification of “a posteriori” method

Firstly, the focus was on the “a posteriori” method. The analysis has been done comparing the signal coming from the ROIs and the signal coming from GM not included in the network. The hypothesis was that the signal coming from the ROIs was higher than the one coming from the outside of the ROIs. So, a cluster-based permutation test with dependent samples T-statistic was performed. In particular, the following parameters has been set:

- **Alpha** (**α**): probability to reject the null hypothesis, 0.05;
- **Tail**: one-tailed, right, because of the initial hypothesis;
- **Method**: Montecarlo;
- **Multiple correction**: cluster;
- **Cluster-alpha**: threshold significance level used for defining clusters, 0.05;

- **Cluster statistic**: “maxsum”, combining the individual samples of a cluster by summing the intensities of all the voxels within that cluster.

The figure 4.1.1 shows the activation signal with the standard error from the all ROIs and from the GM which is not included in these regions (labeled as “Out gray”). It is evident that the ROIs signal is higher than the out gray signal, and this fact is confirmed by the cluster based analysis. Infact, four significant positive clusters were identified (p=0.01, p=0.017, p=0.019, p=0.037), with the time interval that covers nearly the entire period of analysis. The time interval for each clusters (indicated with black dotted line) are the following:

- Cluster 1: 0.0017-0.091 s;
- Cluster 2: 0.114-0.19 s;
- Cluster 3: 0.199-0.2526 s;
- Cluster 4: 0.26-0.35 s.

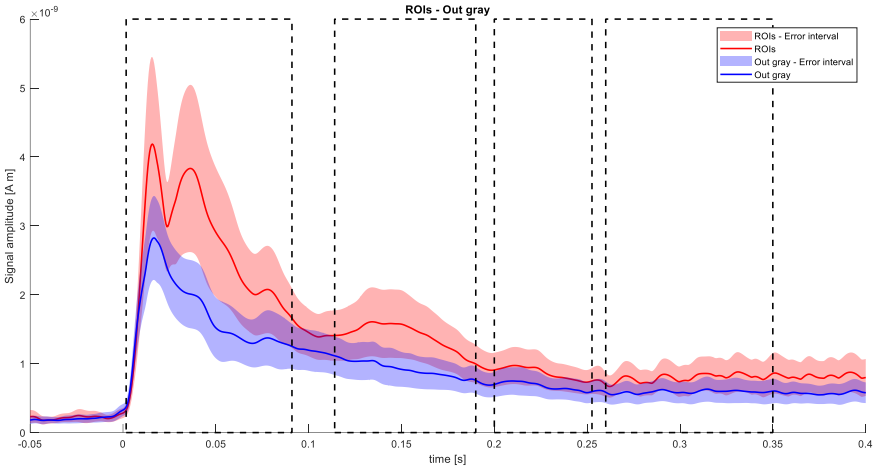

Figure 4.1.1: amplitude signal from ROIs and from the outside grey matter

This was the first essential verification, as without it, the hypothesis that the activation of structurally connected areas is greater than those outside the considered network would not have been confirmed. The results validated that the method was correctly implemented. These clusters indicate that the signal from the ROIs was stronger than that from grey areas outside the network.

To ensure comparability, it was necessary to calculate the z-scores of these values, as the signal obtained from the "a priori" method was two orders of magnitude higher than that from the "a posteriori" method due to physical constraints.

4.2 Main effect of the method

This analysis aimed to examine the **main effect of the method**. Specifically, it compared the activation signals from all ROIs across the two models to determine whether each method produced significantly different outcomes in terms of activation signal amplitude. The same statistical test (cluster based permutation test with dependent samples T-statistic) was applied like in the previous analysis, using the same parameters and procedures. However, in this case, and in the analysis of the next sections as well, the test was two-sided, as there was no initial hypothesis regarding the direction of the effect.

The figure 4.2.1 shows the activation signal from all the ROIs of the network from each method. As shown, no substantial differences are observed, a finding supported by the analysis, which did not identify any significant clusters.

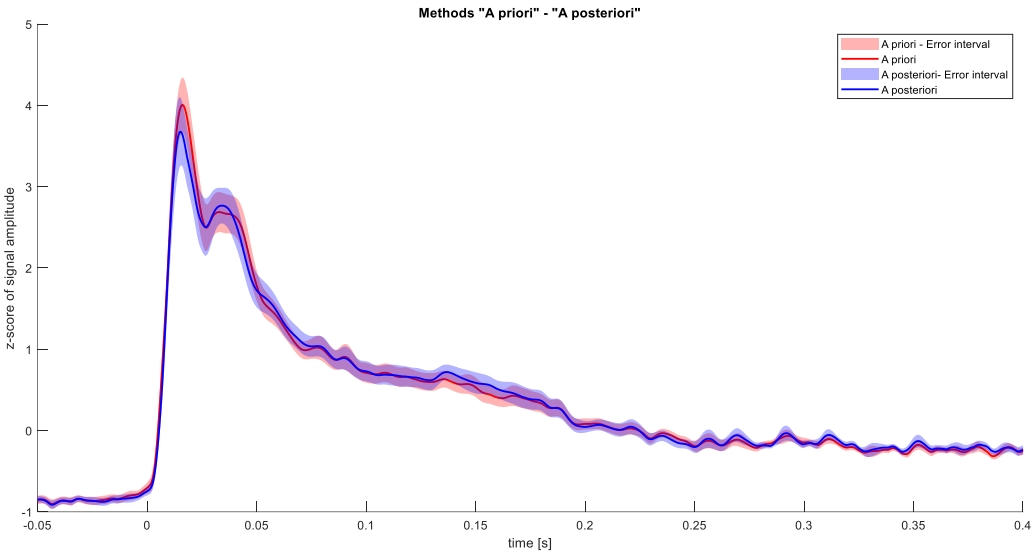

Figure 4.2.1: amplitude signal (z-scored) from the ROIs with both the methods

The purpose of this analysis was to assess how each method influences the results and whether there are significant differences when one method is applied over the other,

considering all the ROIs of the network. The results revealed no significant variations, indicating that within the network, there is no difference between the two methods. This led to the conclusion that both methods perform similarly when considering the entire network.

4.3 Main effect of the ROIs

This analysis focused on examining the **main effect of the ROIs.** It was studied whether, and how, the outcome varied across ROIs, regardless of the model used**.** This began with a cluster-based permutation test using a univariate repeated-measures ANOVA, conducted as a two-sided test. The analysis took in consideration the mean signal between the two methods. To make the results clearer, it is important to remember that ROI 1 and ROI 2 correspond to the regions in the cerebellum. ROI 6 corresponds to the contralateral region on the right hemisphere, ROI 7 corresponds to the stimulated region on the left hemisphere, and ROI 3 corresponds to an area located under ROI 7.

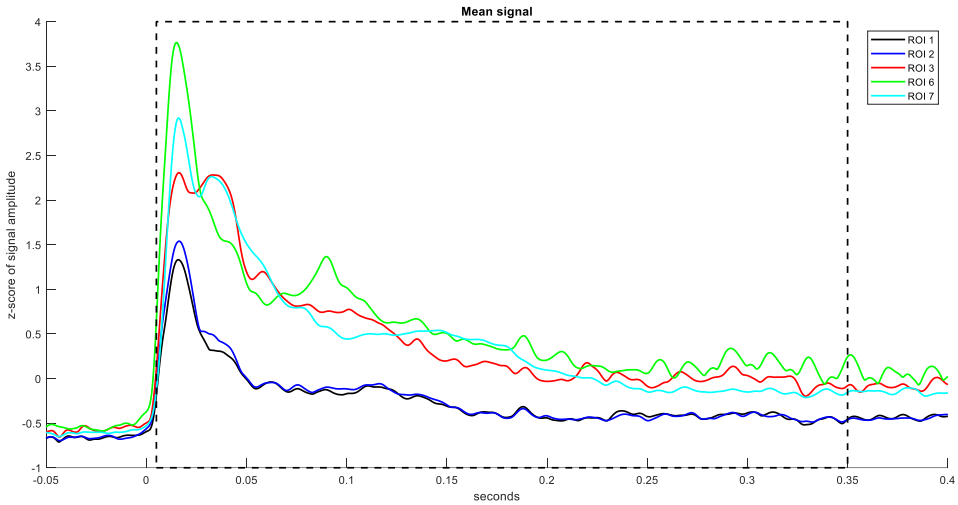

Figure 4.3.1: mean signal (zscored) of the different ROIs

The figure 4.3.1 shows the activation signal from the five different ROIs. The ANOVA test revealed a significant positive cluster spanning the entire time interval of the analysis ($p<0.01$). This implies that the activation signals across the ROIs differ significantly, suggesting a broad pattern of activation throughout the analysis period. To further investigate where these differences lie, pairwise comparisons were conducted between each

of the five ROIs. Specifically, ten separate cluster-based permutation tests with dependent t-tests were performed to determine which regions had significant differences in activation. The graphs and results of each test are shown below, providing a detailed view of the pairwise comparisons between the ROIs.

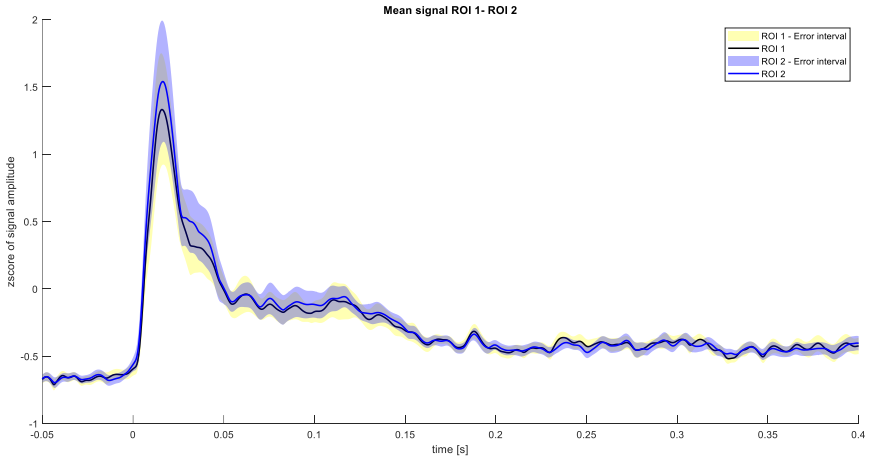

Figure 4.3.2: mean signal (zscored) between ROI 1 and ROI 2

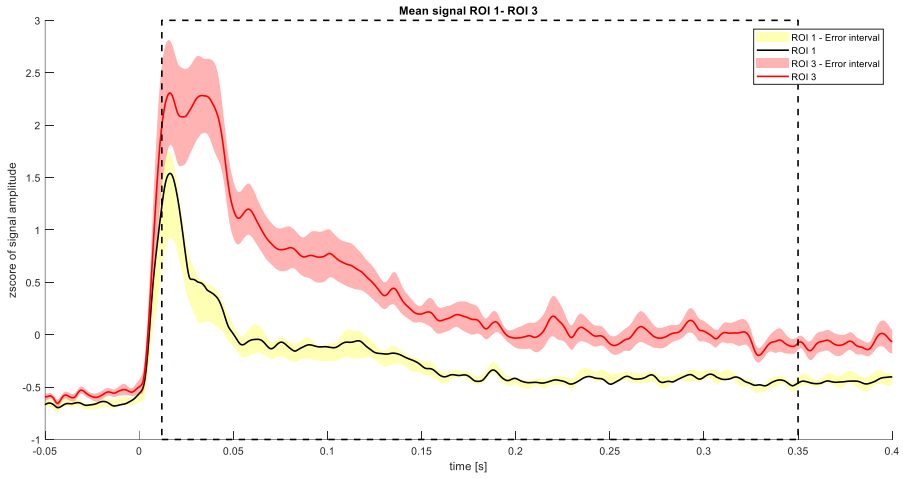

Figure 4.3.3: mean signal (zscored) between ROI 1 and ROI 3

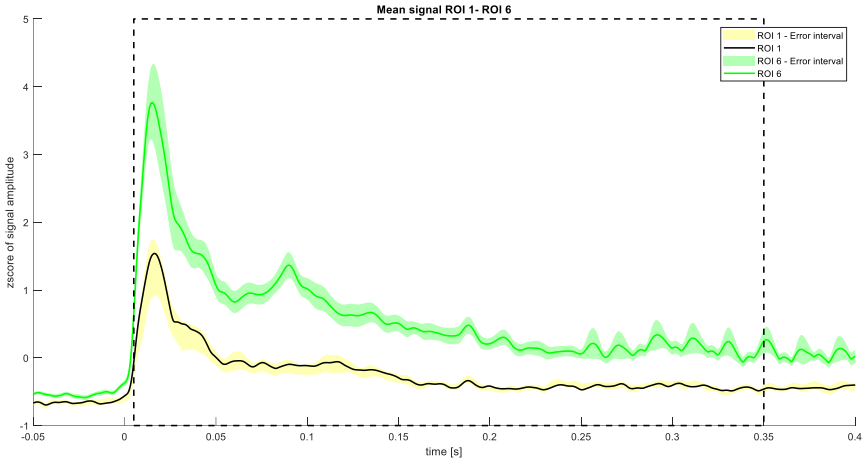

Figure 4.3.4: mean signal (zscored) between ROI 1 and ROI 6

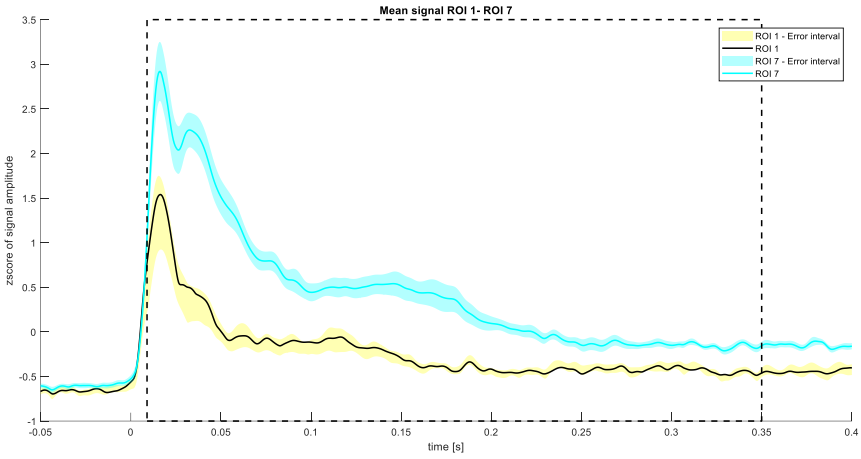

Figure 4.3.5: mean signal (zscored) between ROI 1 and ROI 7

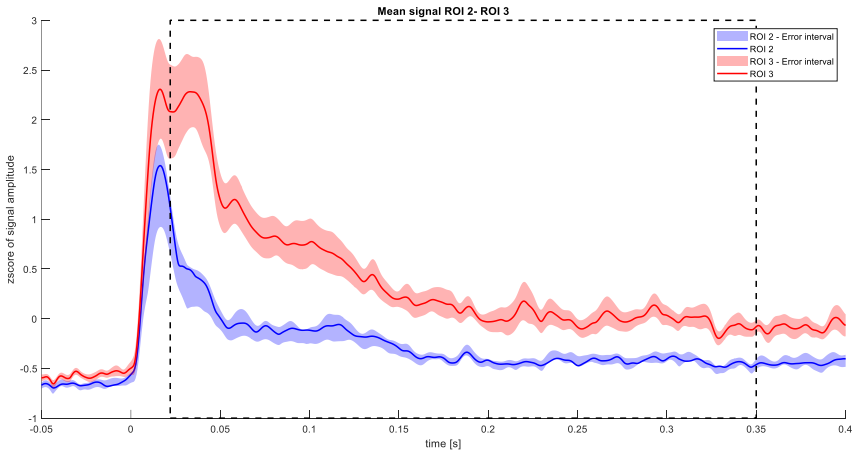

Figure 4.3.6: mean signal (zscored) between ROI 2 and ROI 3

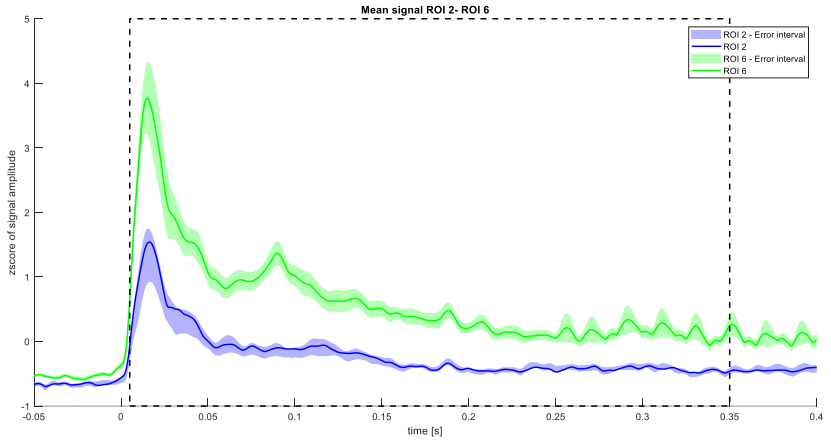

Figure 4.3.7: mean signal (zscored) between ROI 2 and ROI 6

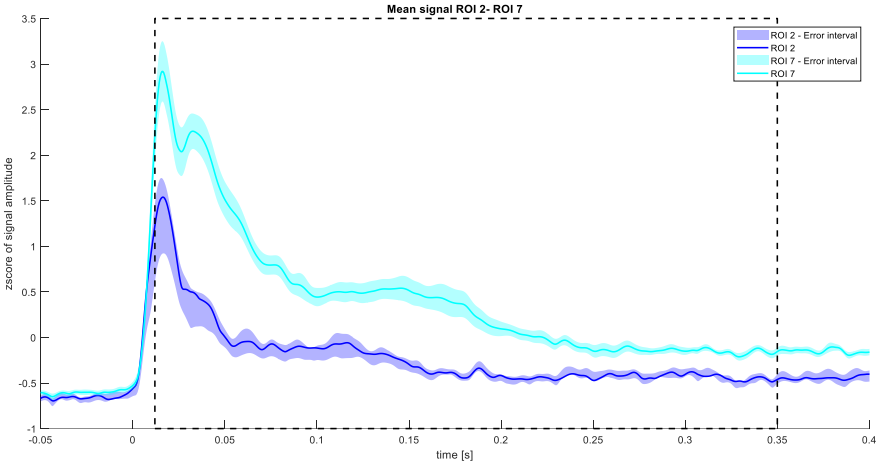

Figure 4.3.8: mean signal (zscored) between ROI 2 and ROI 7

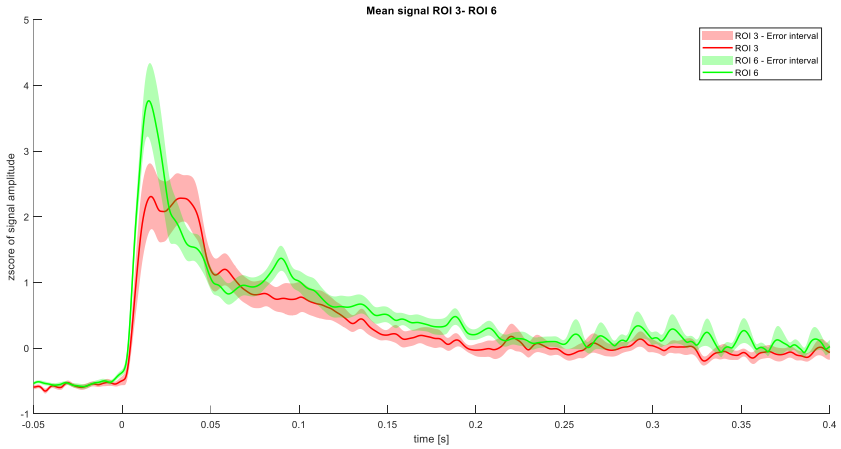

Figure 4.3.9: mean signal (zscored) between ROI 3 and ROI 6

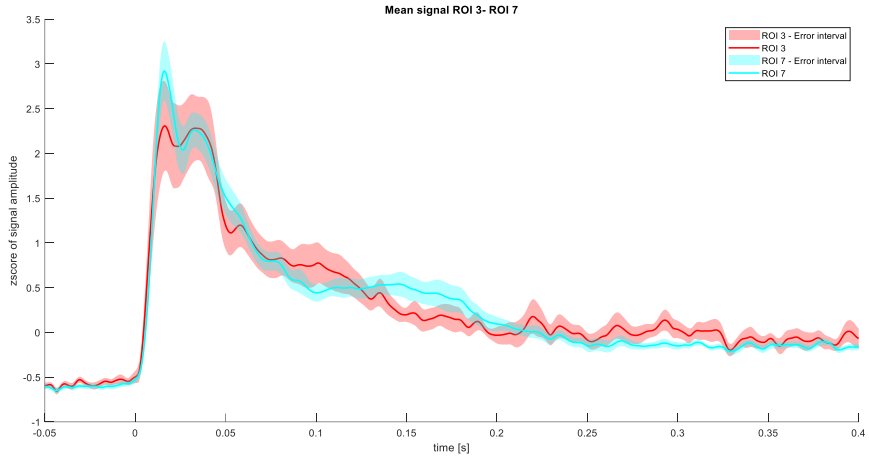

Figure 4.3.10: mean signal (zscored) between ROI 3 and ROI 7

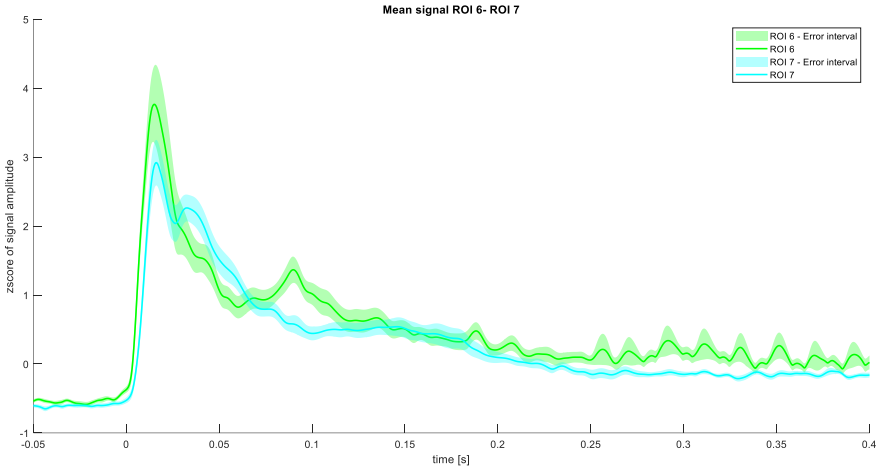

Figure 4.3.11: mean signal (zscored) between ROI 6 and ROI 7

The results from the analysis are reported here:

- ROI 1- ROI 2: no significant clusters (figure 4.3.2);
- ROI 1- ROI 3: one significant negative cluster in almost the whole time (p= 0.02, [0.020-0.35 s]) (figure 4.3.3);
- ROI 1- ROI 6: one significant negative cluster in the whole time interval (p=0.002) (figure 4.3.4);
- ROI 1- ROI 7: one significant negative in almost the whole time interval (p=0.002,[0.009-0.35 s]) (figure 4.3.5);
- ROI 2- ROI 3: one significant negative cluster in almost the whole time interval (p=0.002, [0.022-0.35 s]) (figure 4.3.6);

- ROI 2- ROI 6: one significant negative cluster in the whole time interval (p=0.002) (figure 4.3.7);
- ROI 2- ROI 7: one significant negative cluster in almost the whole time interval (p=0.002,[0.012-0.35 s]) (figure 4.3.8);
- ROI 3- ROI 6: no significant clusters (figure 4.3.9);
- ROI 3- ROI 7: no significant clusters (figure 4.3.10);
- ROI 6- ROI 7: no significant clusters (figure 4.3.11).

From these results it appears that, regardless of the method used, the activation within the cerebellum (ROI 1- ROI 2) appears similar, but significantly different from that measured in ROI 3, ROI 6, ROI 7, which appear to have similar values.

4.4 ROIs-method interaction

The third analysis examined the interaction between **ROI** and **method**. In this case, the analysis considered the difference in signal between the two methods (a priori-a posteriori) and compared this measure between the ROIs. A post-hoc analysis was then performed, comparing the signal of the two methods for each ROI. First, a cluster-based permutation test was conducted, using a univariate repeated-measures ANOVA.

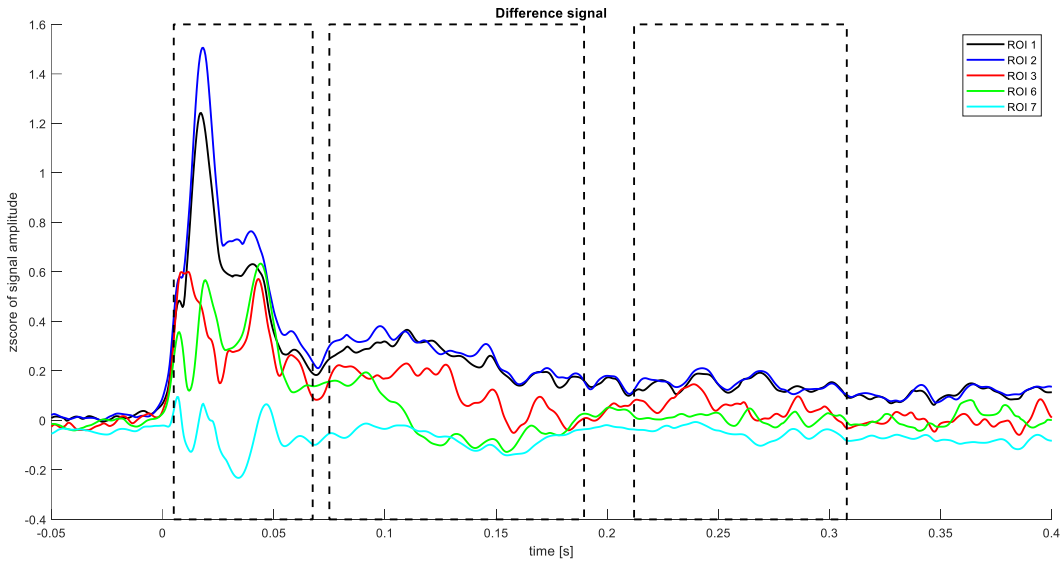

Figure 4.4.1: difference signal (zscored) of each ROIs

The ANOVA test revealed 3 significant positive cluster spanning almost the entire time interval of the analysis ($p<0.05$). This suggests that the two methods are not identical in how they capture the activation signal across the different ROIs. Therefore, it was necessary to

refine the analysis by conducting pairwise comparisons between each of the five ROIs. To achieve this, ten separate cluster-based permutation tests with dependent t-tests were performed. The graphs and results of each test are shown below, providing a detailed view of the pairwise comparisons between the ROIs.

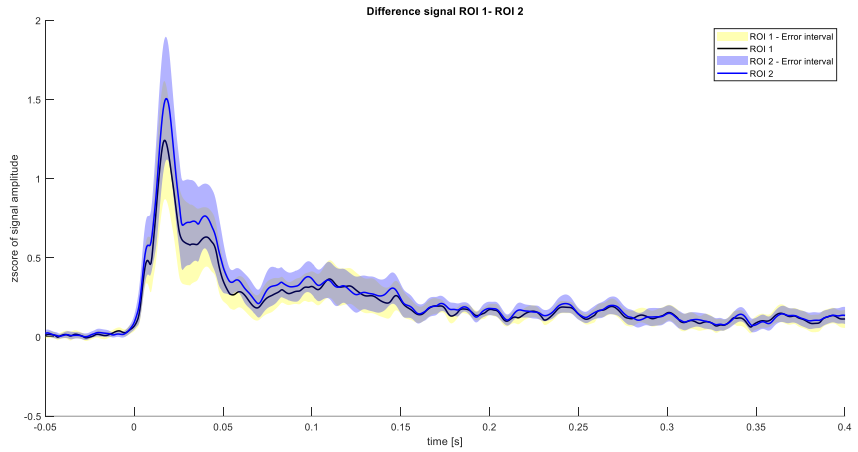

Figure 4.4.2: difference signal (zscored) between ROI 1 and ROI 2

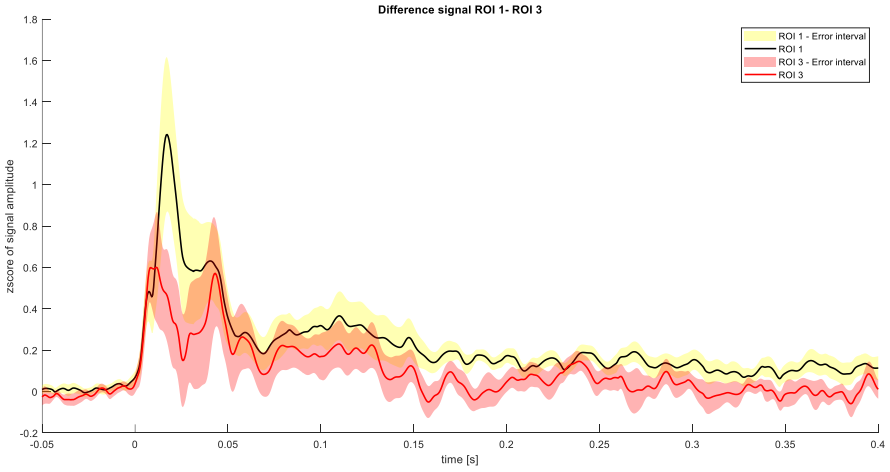

Figure 4.4.3: difference signal (zscored) between ROI 1 and ROI 3

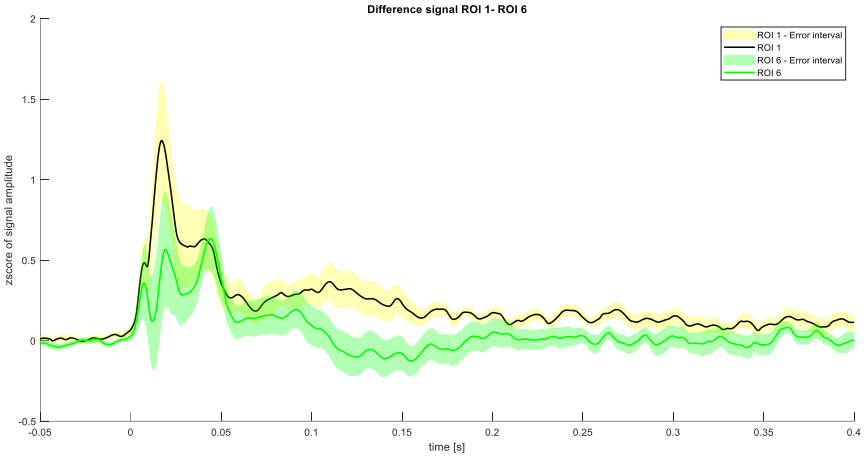

Figure 4.4.4: difference signal (zscored) between ROI 1 and ROI 6

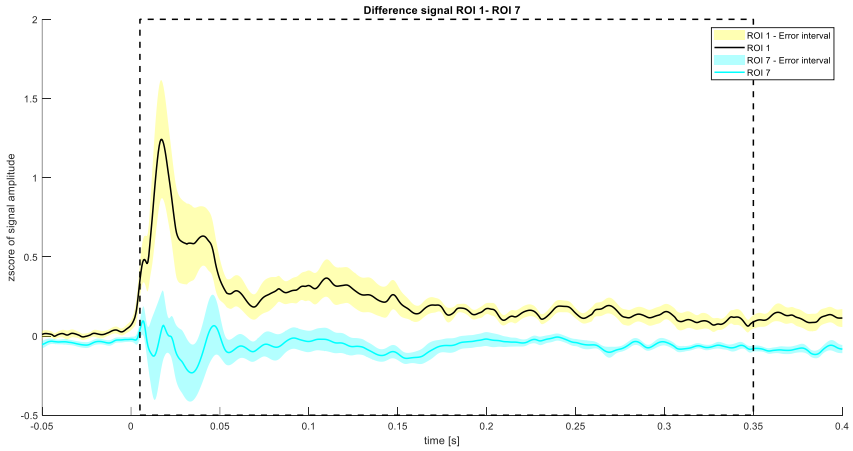

Figure 4.4.5: difference signal (zscored) between ROI 1 and ROI 7

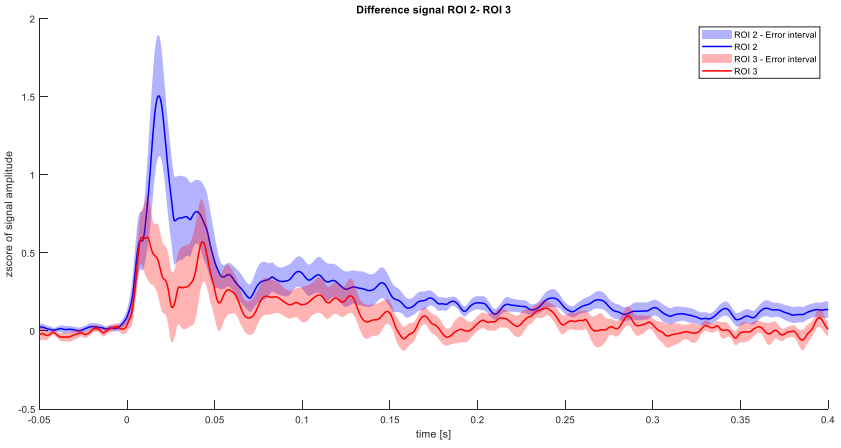

Figure 4.4.6: difference signal (zscored) between ROI 2 and ROI 3

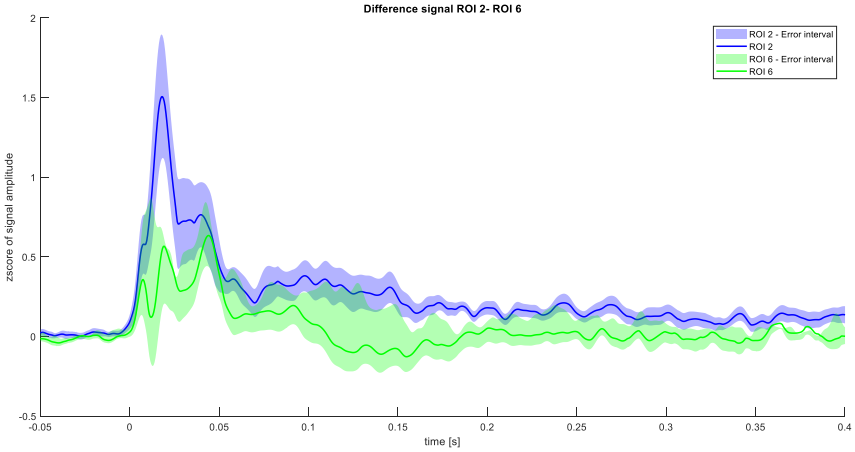

Figure 4.4.7: difference signal (zscored) between ROI 2 and ROI 6

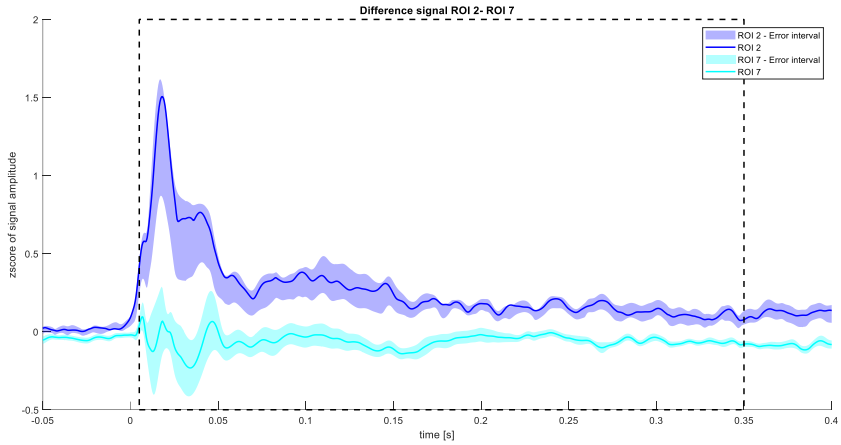

Figure 4.4.8: difference signal (zscored) between ROI 2 and ROI 7

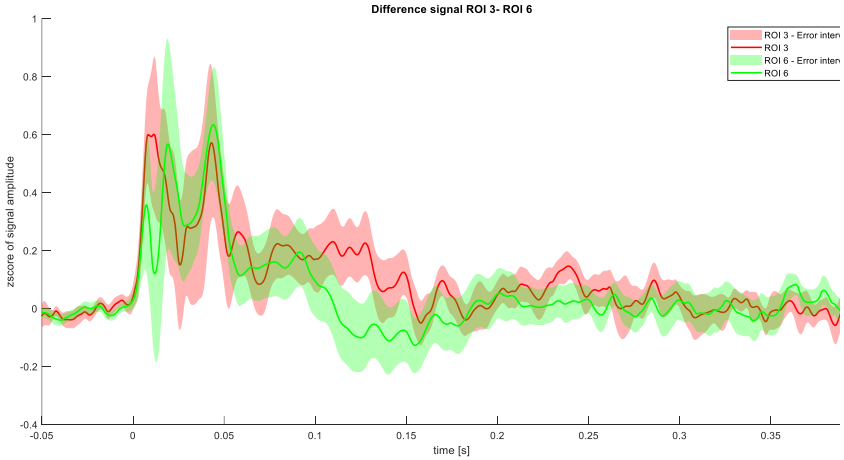

Figure 4.4.9: difference signal (zscored) between ROI 3 and ROI 6

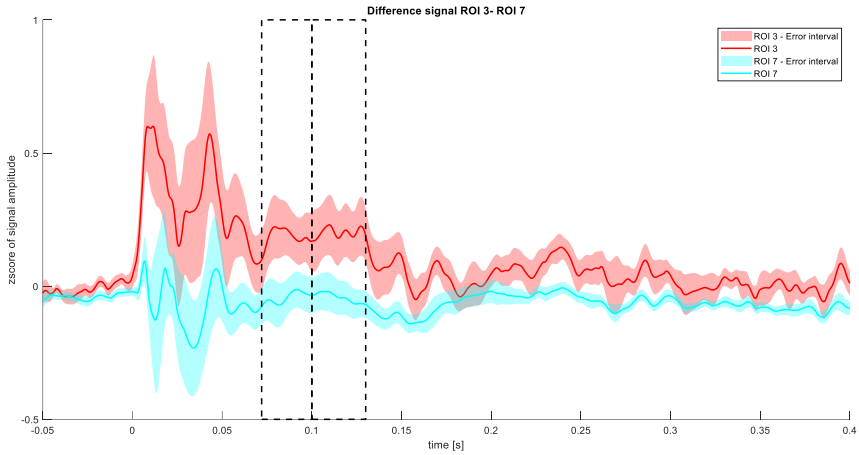

Figure 4.4.10: difference signal (zscored) between ROI 3 and ROI 7

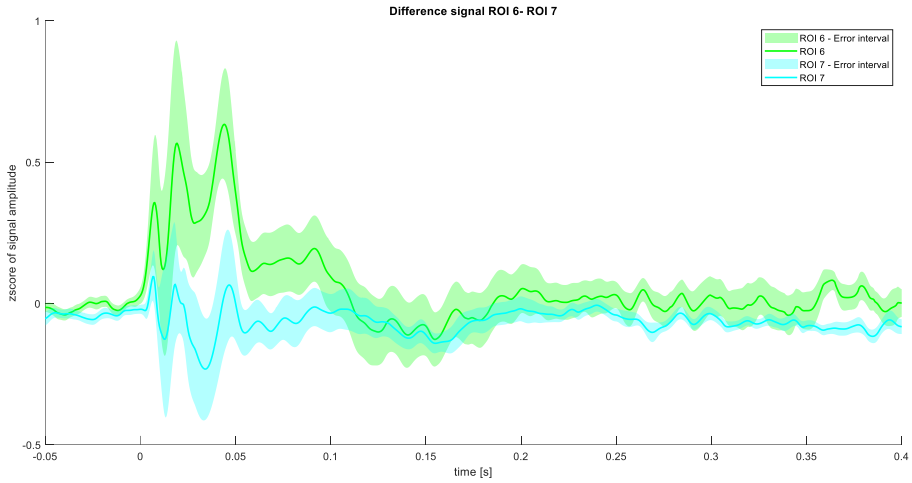

Figure 4.4.11: difference signal (zscored) between ROI 6 and ROI 7

The results from the analysis are reported here:

- ROI 1- ROI 2: no significant clusters (figure 4.4.2);
- ROI 1- ROI 3: no significant clusters (figure 4.4.3);
- ROI 1- ROI 6: no significant clusters (figure 4.4.4);
- ROI 1- ROI 7: one significant positive cluster in the whole time interval (p=0.02) (figure 4.4.5);
- ROI 2- ROI 3: no significant clusters (figure 4.4.6);
- ROI 2- ROI 6: no significant clusters (figure 4.4.7);
- ROI 2- ROI 7: one significant positive cluster in the whole time interval (p=0.02) (figure 4.4.8);
- ROI 3- ROI 6: no significant clusters (figure 4.4.9);

- ROI 3- ROI 7: two significant positive clusters (p=0.046, [0.072-0.133 s] (figure 4.4.10);
- ROI 6- ROI 7: no significant clusters (*one positive cluster with p=0.07 [0.024-0.053 s]) (figure 4.4.11).

These findings suggest that in the cerebellum regions (ROI 1 and ROI 2) the new method seems to explain a stronger activation, indicating a more pronounced effect.

In the post-hoc analysis, five separate cluster-based permutation tests, using dependent t-tests were computed. Each test compared the signal between the "a priori" and "a posteriori" methods within each ROI.

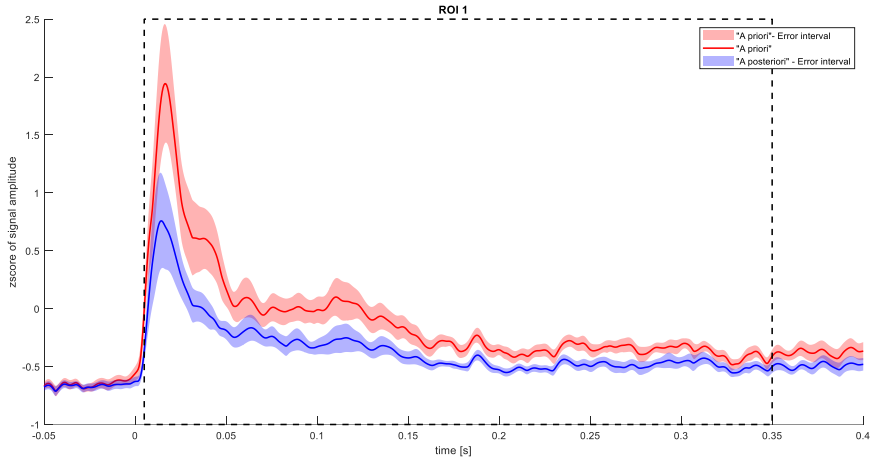

Figure 4.4.12: amplitude signal (zscored) from the different methods in ROI 1

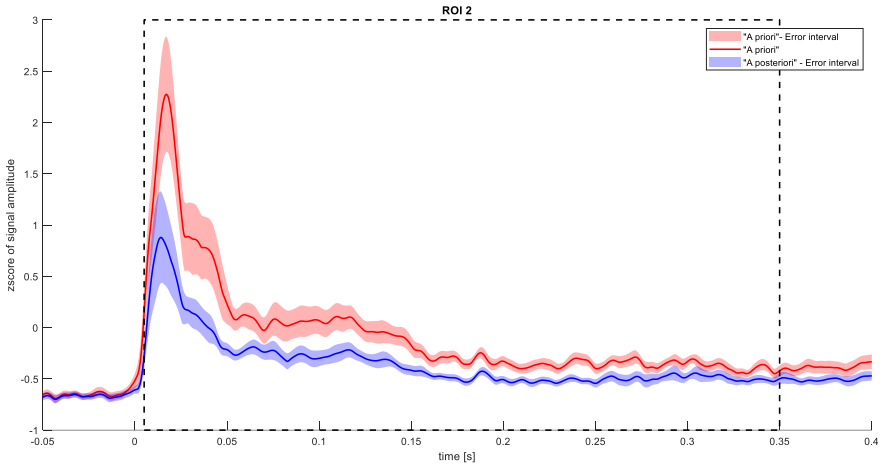

Figure 4.4.13: amplitude signal (zscored) from the different methods in ROI 2

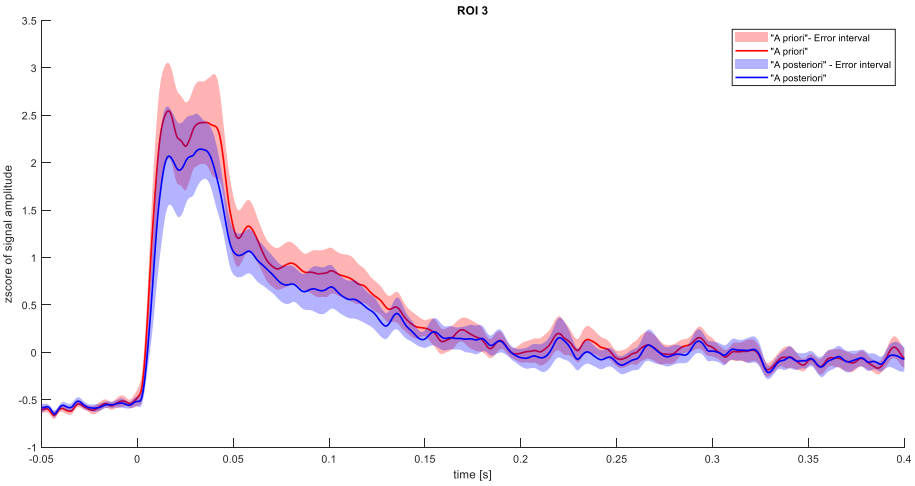

Figure 4.4.14: amplitude signal (zscored) from the different methods in ROI 3

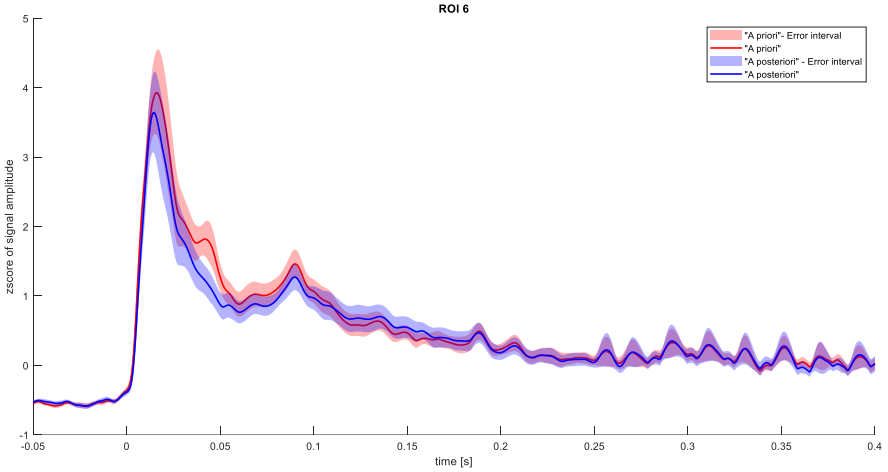

Figure 4.4.15: amplitude signal (zscored) from the different methods in ROI 6

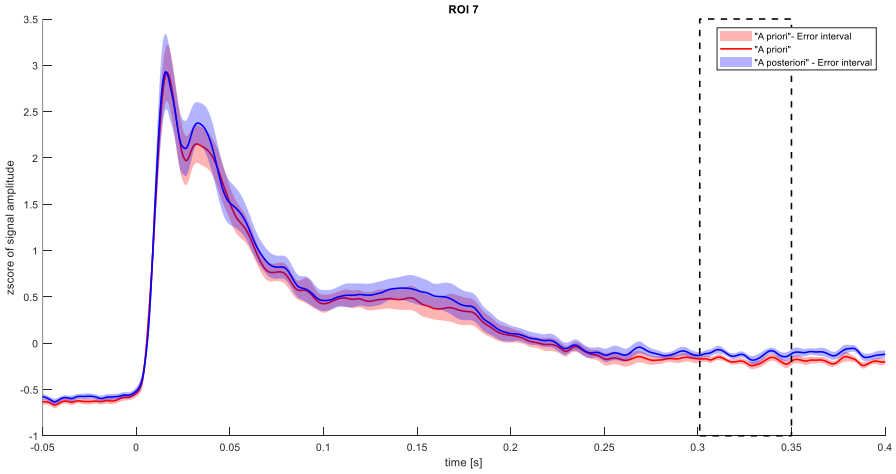

Figure 4.4.16: amplitude signal (zscored) from the different methods in ROI 7

The results from the analysis are reported here:

- ROI 1: one significant postive cluster (p=0.002, [0.005-0.306s]) (figure 4.4.12)
- ROI 2: one significant positive cluster (p=0.002, [0.005-0.306 s]) (figure 4.4.13)
- ROI 3: no significant clusters (figure 4.4.14);
- ROI 6: no significant clusters (figure 4.4.15);
- ROI 7: one significant negative cluster (p=0.002, [0.301-0.35 s]) (*one negative cluster p=0.067,[0.135-0.166 s]) (figure 4.4.16).

The results from this analysis shows in both ROI 1 and ROI 2 significant positive clusters for the time period between 0.005-0.30 seconds. No significant clusters were found in the remaining ROIs, except for one negative cluster in ROI 7 for a few milliseconds. This results are in line with the findings from the previous section, and can lead to the conclusion that the "A priori" method produces different results in the cerebellar regions but not in the others regions.

5. Discussion

In this section I will present the discussion, analysing the results, the limitations, and the implications of the research project. From these results it possible to conclude that:

1. The activation of the brain network stimulated is higher than the rest of the GM;
2. The new method performs similarly to the previous one in the overall analysis of the network, showing comparable performance;
3. The activation is primarily detected in the stimulated area, the adjacent area and the contralateral region, which presents similar values, while is significantly reduced in the cerebellar regions;
4. When focusing on the specific regions, the new method reveals a significant difference by detecting stronger activation in the cerebellum compared to the previous method. This suggests that the "A priori" model has greater sensitivity in cerebellar regions.

As expected, the activation of the entire network produces a higher signal compared to the rest of the GM. Additionally, as hypothesized, the signal from ROI 6-7-3 (stimulated and controlateral region) is higher than the one in ROI 1-2 (cerebellum), due to physical distance and weaker connections. Moreover, it was observed that the contralateral region activated concurrently with the ipsilateral region, which is in line with recent findings in the literature [26].

However, the pipeline used in this project has been carefully selected and designed to ensure robust and reliable analysis. The approach implemented in this analysis is both reasonable and consistent with existing literature. Furthermore, the results obtained from this method were compared with those obtained from the LORETA software, a widely used tool in neuroimaging. This comparison further supports the reliability of the results.

A possible reason why no major differences were observed between the two methods, except in the cerebellum, could lie in a technical aspect of both models implemented. Typically, the segmentation approach used is the boundary element model (BEM) [33], but in this case the finite element model (FEM) was used for both models. This choice was made based on the default settings of FieldTrip [56] which are intended to provide a more accurate estimation compared to the BEM model [67]. As a result, the 'A posteriori' model is likely already performing well across most regions, which may explain the lack

of substantial differences in most areas.

An important consideration can be made regarding the role of the cerebellum. The results of this study align with recent literature suggesting that cerebellar activity, contrary to past assumptions, can be effectively detected using EEG and MEG, particularly when appropriate source reconstruction methods are employed [72]. Some difficulties in detecting cerebellar signals born from its anatomical structure, which can cause signal cancellation due to opposing current flows in adjacent sulci. Additionally, cerebellar activity is characterized by less synchronous and more localized oscillations compared to the cerebral cortex, making it harder to capture with traditional EEG methods designed for capturing phase-locked signals. The improved sensitivity of the 'a priori' method compared to the other may be explained by the intrinsic approach implemented. This tailored approach accounts for the cerebellum's activity, enabling more accurate detection of its signals. By explicitly incorporating these regions into the model, the 'a priori' method seems to overcome these limitations and explains cerebellar activity more effectively.

Based on these results, it would be interesting to investigate how the new method performs in the ROIs that were excluded from the analysis (ROI 4 and ROI 5). The exclusion of these regions is justified by their absence in two subjects, which is due to a combination of factors related to both implementation choices and the construction of the source model.

Some considerations can be made about the implementation choices of the two methods. Initially, it has been necessary to understand which steps were required for the process of source reconstruction using the software-toolbox FieldTrip [56]. The choice of this software is justified because of its flexibility, which allows it to adapt to various analysis needs and applications in the field of neuroscience. Each step, as presented in the Methods chapter, was conducted according to FieldTrip guidelines [67], supported by the literature, and carefully evaluated for its suitability to our specific research needs. The first steps of the pipeline involved several passages in order to use the standard template, aligning the two volumes and obtaining the ROIs[9]. As previously mentioned, the initial idea was to use individual tractography to preserve the individual characteristics of each subject, i.e. their structural connectivity. However, due to technical issues, it was not possible to exploit this measure, and therefore the use of a template became necessary. In this way, a degree of standardization has been introduced, but with the advantages of combining two neuroimaging techniques: the fMRI and the DTI. In fact, the extracted template combined the functional and structural connectivity, respectively. This approach, while introducing a

degree of standardization, allows for the exploration of results while accounting for inter-individual variability.

For the choice of the algorithm of source reconstruction, MNE has been selected, following the state-of-the-art approach for the “a posterior” model. For the other model, we initially hypothesized that an ECD approach might be more suitable. However, the numerous ROIs and the extent of the areas made this approach difficult to implement effectively. Future studies could further explore the influence of parameters within the algorithm, such as the lambda measure and SNR values, to assess their impact on performance.

An interesting direction for future research involves the use of the software SimNIBS (Stimulation of Non-Invasive Brain Stimulation) [73], an open-source software package designed to simulate non-invasive brain stimulation. This software enables realistic calculation of the electric field induced by TMS, allowing researchers to accurately identify the areas affected by the stimulation. By integrating this information with a composite map of structural MRI and template-based fMRI-DTI, it would be possible to select the regions with the strongest stimulation effect. This integration could potentially make it feasible to use ECD model, as smaller and more localized regions better align with this method’s requirements. This integration could potentially help to better understand TMS's impact on targeted brain areas and their connections and so improve TEP source localization accuracy.

From a computational perspective, the new method seems to be more efficient as it reduces the computational cost. Specifically, the calculation of the source model and lead field is less demanding, due to the substantial reduction in the number of source locations, from approximately 4000 to 140.

Beyond technical considerations, the results of this study could have potential implications for patient population, particularly those with damaged structural connectivity or altered brain network patterns. The integration of functional and structural imaging data, as demonstrated in this study, offers a more targeted and personalised approach to understanding brain activity in healthy subjects. This approach could be useful in the design of individualised rehabilitation or therapeutic interventions. For instance, for MS pathology, this can be applied leading to the development of therapeutic interventions to support neuroplasticity.

6.Conclusion

This study aimed to develop and evaluate a new TEP source reconstruction method. The results showed that, overall, the new method did not perform differently from the traditional approach in terms of activation of the entire network. However, when examining specific regions, the new method revealed significantly higher levels of activity in the cerebellum than the other method. The ‘a priori’ method seems to be able to overcome the limitations associated with detecting the EEG signal from regions of the cerebellum. However, the study has some limitations that could be object of future studies.

In summary, this study illustrates the potential of the new source reconstruction method to advance our understanding of brain activity, especially in under studied regions such as the cerebellum. By enabling a more accurate localization of brain activity, it could improve both research and clinical applications, leading to more targeted and effective treatments for individuals with altered brain network patterns or anatomical structures.

Bibliography

[1] D. U. Silverthorn, *Human Physiology: An Integrated Approach*, 7th edition. Pearson, 2015.

[2] «National Institutes of Health (NIH)», National Institutes of Health (NIH). Consultato: 1 agosto 2024. [Online]. Disponibile su: https://www.nih.gov/

[3] M. S. Gazzaniga, «Cerebral specialization and interhemispheric communication: does the corpus callosum enable the human condition?», *Brain*, vol. 123 (Pt 7), pp. 1293–1326, lug. 2000, doi: 10.1093/brain/123.7.1293.

[4] J. Tomasch, «Size, distribution, and number of fibres in the human corpus callosum», *Anat Rec*, vol. 119, fasc. 1, pp. 119–135, mag. 1954, doi: 10.1002/ar.1091190109.

[5] D. Rong, M. Zhang, Q. Ma, J. Lu, e K. Li, «Corticospinal Tract Change during Motor Recovery in Patients with Medulla Infarct: A Diffusion Tensor Imaging Study», *Biomed Res Int*, vol. 2014, p. 524096, 2014, doi: 10.1155/2014/524096.

[6] M. D. Fox, A. Z. Snyder, J. L. Vincent, M. Corbetta, D. C. Van Essen, e M. E. Raichle, «The human brain is intrinsically organized into dynamic, anticorrelated functional networks», *Proc Natl Acad Sci U S A*, vol. 102, fasc. 27, pp. 9673–9678, lug. 2005, doi: 10.1073/pnas.0504136102.

[7] J. S. Damoiseaux *et al.*, «Consistent resting-state networks across healthy subjects», *Proc Natl Acad Sci U S A*, vol. 103, fasc. 37, pp. 13848–13853, set. 2006, doi: 10.1073/pnas.0601417103.

[8] B. T. T. Yeo *et al.*, «The organization of the human cerebral cortex estimated by intrinsic functional connectivity», *J Neurophysiol*, vol. 106, fasc. 3, pp. 1125–1165, set. 2011, doi: 10.1152/jn.00338.2011.

[9] V. Nozais *et al.*, «Atlasing white matter and grey matter joint contributions to resting-state networks in the human brain», *Commun Biol*, vol. 6, fasc. 1, pp. 1–11, lug. 2023, doi: 10.1038/s42003-023-05107-3.

[10] M. Bortoletto e C. Miniussi, «Integrating TMS, EEG, and MRI as an Approach for Studying Brain Connectivity», *Neuroscientist*, vol. 26, fasc. 5–6, pp. 471–486, 2020, doi: 10.1177/1073858420916452.

[11] O. Sporns, «The human connectome: a complex network», *Ann N Y Acad Sci*, vol. 1224, pp. 109–125, apr. 2011, doi: 10.1111/j.1749-6632.2010.05888.x.

[12] C. J. Honey, J.-P. Thivierge, e O. Sporns, «Can structure predict function in the human brain?», *Neuroimage*, vol. 52, fasc. 3, pp. 766–776, set. 2010, doi: 10.1016/j.neuroimage.2010.01.071.

[13] P. Babaeeghazvini, L. M. Rueda-Delgado, J. Gooijers, S. P. Swinnen, e A. Daffertshofer, «Brain Structural and Functional Connectivity: A Review of Combined Works of Diffusion Magnetic Resonance Imaging and Electro-Encephalography», *Front. Hum. Neurosci.*, vol. 15, ott. 2021, doi: 10.3389/fnhum.2021.721206.

[14] M. Bortoletto, D. Veniero, G. Thut, e C. Miniussi, «The contribution of TMS–EEG coregistration in the exploration of the human cortical connectome», *Neuroscience & Biobehavioral Reviews*, vol. 49, pp. 114–124, feb. 2015, doi: 10.1016/j.neubiorev.2014.12.014.

[15] R. Esposito, M. Bortoletto, D. Zacà, P. Avesani, e C. Miniussi, «An integrated TMS-EEG and MRI approach to explore the interregional connectivity of the default mode network», *Brain Struct Funct*, vol. 227, fasc. 3, pp. 1133–1144, apr. 2022, doi: 10.1007/s00429-022-02453-6.

[16] R. J. Ilmoniemi, J. Ruohonen, e J. Karhu, «Transcranial magnetic stimulation--a new tool for functional imaging of the brain», *Crit Rev Biomed Eng*, vol. 27, fasc. 3–5, pp. 241–284, 1999.

[17] E. D. Adrian e G. Moruzzi, «Impulses in the pyramidal tract», *The Journal of Physiology*, vol. 97, fasc. 2, pp. 153–199, 1939, doi: 10.1113/jphysiol.1939.sp003798.

[18] A. T. Barker, R. Jalinous, e I. L. Freeston, «NON-INVASIVE MAGNETIC STIMULATION OF HUMAN MOTOR CORTEX», *The Lancet*, vol. 325, fasc. 8437, pp. 1106–1107, mag. 1985, doi: 10.1016/S0140-6736(85)92413-4.

[19] C. Bonato, C. Miniussi, e P. M. Rossini, «Transcranial magnetic stimulation and cortical evoked potentials: a TMS/EEG co-registration study», *Clin Neurophysiol*, vol. 117, fasc. 8, pp. 1699–1707, ago. 2006, doi: 10.1016/j.clinph.2006.05.006.
[20] J.-P. Lefaucheur *et al.*, «Evidence-based guidelines on the therapeutic use of repetitive transcranial magnetic stimulation (rTMS)», *Clin Neurophysiol*, vol. 125, fasc. 11, pp. 2150–2206, nov. 2014, doi: 10.1016/j.clinph.2014.05.021.
[21] P. S. Tofts, «The distribution of induced currents in magnetic stimulation of the nervous system», *Phys. Med. Biol.*, vol. 35, fasc. 8, p. 1119, ago. 1990, doi: 10.1088/0031-9155/35/8/008.
[22] W. Klomjai, R. Katz, e A. Lackmy-Vallée, «Basic principles of transcranial magnetic stimulation (TMS) and repetitive TMS (rTMS)», *Annals of Physical and Rehabilitation Medicine*, vol. 58, fasc. 4, pp. 208–213, set. 2015, doi: 10.1016/j.rehab.2015.05.005.
[23] A. Biasiucci, B. Franceschiello, e M. M. Murray, «Electroencephalography», *Current Biology*, vol. 29, fasc. 3, pp. R80–R85, feb. 2019, doi: 10.1016/j.cub.2018.11.052.
[24] X. Jiang, G.-B. Bian, e Z. Tian, «Removal of Artifacts from EEG Signals: A Review», *Sensors (Basel)*, vol. 19, fasc. 5, p. 987, feb. 2019, doi: 10.3390/s19050987.
[25] R. J. Ilmoniemi *et al.*, «Neuronal responses to magnetic stimulation reveal cortical reactivity and connectivity», *Neuroreport*, vol. 8, fasc. 16, pp. 3537–3540, nov. 1997, doi: 10.1097/00001756-199711100-00024.
[26] M. Bortoletto *et al.*, «Asymmetric transcallosal conduction delay leads to finer bimanual coordination.», *Brain Stimul*, vol. 14, fasc. 2, pp. 379–388, apr. 2021, doi: 10.1016/j.brs.2021.02.002.
[27] A. Zazio, G. Barchiesi, C. Ferrari, E. Marcantoni, e M. Bortoletto, «M1-P15 as a cortical marker for transcallosal inhibition: A preregistered TMS-EEG study», *Front Hum Neurosci*, vol. 16, p. 937515, set. 2022, doi: 10.3389/fnhum.2022.937515.
[28] J. C. Hernandez-Pavon *et al.*, «TMS combined with EEG: Recommendations and open issues for data collection and analysis», *Brain Stimul*, vol. 16, fasc. 2, pp. 567–593, 2023, doi: 10.1016/j.brs.2023.02.009.
[29] Z.-D. Deng, S. H. Lisanby, e A. V. Peterchev, «Electric field depth-focality tradeoff in transcranial magnetic stimulation: simulation comparison of 50 coil designs», *Brain Stimul*, vol. 6, fasc. 1, pp. 1–13, gen. 2013, doi: 10.1016/j.brs.2012.02.005.
[30] M. C. Romero, M. Davare, M. Armendariz, e P. Janssen, «Neural effects of transcranial magnetic stimulation at the single-cell level», *Nat Commun*, vol. 10, fasc. 1, p. 2642, giu. 2019, doi: 10.1038/s41467-019-10638-7.
[31] A. Valero-Cabré, J. L. Amengual, C. Stengel, A. Pascual-Leone, e O. A. Coubard, «Transcranial magnetic stimulation in basic and clinical neuroscience: A comprehensive review of fundamental principles and novel insights», *Neuroscience & Biobehavioral Reviews*, vol. 83, pp. 381–404, dic. 2017, doi: 10.1016/j.neubiorev.2017.10.006.
[32] R. A. Ozdemir *et al.*, «Individualized perturbation of the human connectome reveals reproducible biomarkers of network dynamics relevant to cognition», *Proc Natl Acad Sci U S A*, vol. 117, fasc. 14, pp. 8115–8125, apr. 2020, doi: 10.1073/pnas.1911240117.
[33] D. Momi *et al.*, «Network-level macroscale structural connectivity predicts propagation of transcranial magnetic stimulation», *NeuroImage*, vol. 229, p. 117698, apr. 2021, doi: 10.1016/j.neuroimage.2020.117698.
[34] D. Momi *et al.*, «Perturbation of resting-state network nodes preferentially propagates to structurally rather than functionally connected regions», *Sci Rep*, vol. 11, fasc. 1, p. 12458, giu. 2021, doi: 10.1038/s41598-021-90663-z.
[35] D. Momi, Z. Wang, e J. D. Griffiths, «TMS-evoked responses are driven by recurrent large-scale network dynamics», *Elife*, vol. 12, p. e83232, apr. 2023, doi: 10.7554/eLife.83232.
[36] M. BRAZIER, «A study of the electrical fields at the surface of the head», *Electro epi Clin Neuro physiol*, vol. 2, pp. 38–52, 1949.

[37] J. Vorwerk, J.-H. Cho, S. Rampp, H. Hamer, T. R. Knösche, e C. H. Wolters, «A guideline for head volume conductor modeling in EEG and MEG», *NeuroImage*, vol. 100, pp. 590–607, ott. 2014, doi: 10.1016/j.neuroimage.2014.06.040.
[38] B. Burle, L. Spieser, C. L. Rogers, L. Casini, T. Hasbroucq, e F. Vidal, «Spatial and temporal resolutions of EEG: Is it really black and white? A scalp current density view», *International Journal of Psychophysiology*, vol. 97, fasc. 3, Art. fasc. 3, set. 2015, doi: 10.1016/j.ijpsycho.2015.05.004.
[39] L. Mainardi e P. Ravazzani, *Principi di bioelettricità e bioelettromagnetismo*. Pàtron, 2011.
[40] O. Hauk, M. Stenroos, e M. S. Treder, «Towards an objective evaluation of EEG/MEG source estimation methods - The linear approach», *Neuroimage*, vol. 255, p. 119177, lug. 2022, doi: 10.1016/j.neuroimage.2022.119177.
[41] J. Sarvas, «Basic mathematical and electromagnetic concepts of the biomagnetic inverse problem», *Phys. Med. Biol.*, vol. 32, fasc. 1, pp. 11–22, gen. 1987, doi: 10.1088/0031-9155/32/1/004.
[42] C. Michel e B. he, «EEG mapping and source imaging», *Niedermeyer's Electroencephalography*, pp. 1179–1202, ott. 2012.
[43] T.-H. Eom, «Electroencephalography source localization», *Clin Exp Pediatr*, vol. 66, fasc. 5, pp. 201–209, dic. 2022, doi: 10.3345/cep.2022.00962.
[44] J. S. Ebersole, «EEG dipole modeling in complex partial epilepsy», *Brain Topogr*, vol. 4, fasc. 2, pp. 113–123, 1991, doi: 10.1007/BF01132768.
[45] M. S. Hämäläinen e R. J. Ilmoniemi, «Interpreting magnetic fields of the brain: minimum norm estimates», *Med Biol Eng Comput*, vol. 32, fasc. 1, pp. 35–42, gen. 1994, doi: 10.1007/BF02512476.
[46] C. M. Michel e D. Brunet, «EEG Source Imaging: A Practical Review of the Analysis Steps», *Front. Neurol.*, vol. 10, apr. 2019, doi: 10.3389/fneur.2019.00325.
[47] F. Lenzen e O. Scherzer, «Tikhonov type regularization methods: History and recent progress», *Proceeding Eccomas*, vol. 2004, gen. 2004.
[48] M. Bertero, C. D. Mol, e E. R. Pike, «Linear inverse problems with discrete data: II. Stability and regularisation», *Inverse Problems*, vol. 4, fasc. 3, p. 573, ago. 1988, doi: 10.1088/0266-5611/4/3/004.
[49] G. H. Golub, M. Heath, e G. Wahba, «Generalized Cross-Validation as a Method for Choosing a Good Ridge Parameter», *Technometrics*, vol. 21, fasc. 2, pp. 215–223, mag. 1979, doi: 10.1080/00401706.1979.10489751.
[50] P. C. Hansen, «Analysis of Discrete Ill-Posed Problems by Means of the L-Curve», *SIAM Review*, vol. 34, fasc. 4, pp. 561–580, 1992.
[51] R. D. Pascual-Marqui, C. M. Michel, e D. Lehmann, «Low resolution electromagnetic tomography: a new method for localizing electrical activity in the brain», *Int J Psychophysiol*, vol. 18, fasc. 1, pp. 49–65, ott. 1994, doi: 10.1016/0167-8760(84)90014-x.
[52] A. M. Dale *et al.*, «Dynamic Statistical Parametric Mapping: Combining fMRI and MEG for High-Resolution Imaging of Cortical Activity», *Neuron*, vol. 26, fasc. 1, pp. 55–67, apr. 2000, doi: 10.1016/S0896-6273(00)81138-1.
[53] R. Grave de Peralta Menendez, M. M. Murray, C. M. Michel, R. Martuzzi, e S. L. Gonzalez Andino, «Electrical neuroimaging based on biophysical constraints», *NeuroImage*, vol. 21, fasc. 2, pp. 527–539, feb. 2004, doi: 10.1016/j.neuroimage.2003.09.051.
[54] D. Veniero, M. Bortoletto, e C. Miniussi, «TMS-EEG co-registration: on TMS-induced artifact», *Clin Neurophysiol*, vol. 120, fasc. 7, pp. 1392–1399, lug. 2009, doi: 10.1016/j.clinph.2009.04.023.
[55] A. Delorme e S. Makeig, «EEGLAB: an open source toolbox for analysis of single-trial EEG dynamics including independent component analysis», *J Neurosci Methods*, vol. 134, fasc. 1, pp. 9–21, mar. 2004, doi: 10.1016/j.jneumeth.2003.10.009.
[56] O. R, F. P, M. E, e S. Jm, «FieldTrip: Open source software for advanced analysis of MEG, EEG, and invasive electrophysiological data», *Computational intelligence and neuroscience*, vol. 2011, 2011, doi: 10.1155/2011/156869.

[57] T. P. Mutanen, J. Metsomaa, S. Liljander, e R. J. Ilmoniemi, «Automatic and robust noise suppression in EEG and MEG: The SOUND algorithm», *Neuroimage*, vol. 166, pp. 135–151, feb. 2018, doi: 10.1016/j.neuroimage.2017.10.021.
[58] T. P. Mutanen, M. Kukkonen, J. O. Nieminen, M. Stenroos, J. Sarvas, e R. J. Ilmoniemi, «Recovering TMS-evoked EEG responses masked by muscle artifacts», *Neuroimage*, vol. 139, pp. 157–166, ott. 2016, doi: 10.1016/j.neuroimage.2016.05.028.
[59] F. Vatta, F. Meneghini, F. Esposito, S. Mininel, e F. D. Salle, «Realistic and Spherical Head Modeling for EEG Forward Problem Solution: A Comparative Cortex-Based Analysis», *Computational Intelligence and Neuroscience*, vol. 2010, p. 972060, feb. 2010, doi: 10.1155/2010/972060.
[60] M. A. Jatoi, N. Kamel, I. Faye, A. Saeed Malik, J. M. Bornot, e T. Begum, «BEM based solution of forward problem for brain source estimation», in *2015 IEEE International Conference on Signal and Image Processing Applications (ICSIPA)*, ott. 2015, pp. 180–185. doi: 10.1109/ICSIPA.2015.7412186.
[61] M. Fuchs, J. Kastner, M. Wagner, S. Hawes, e J. S. Ebersole, «A standardized boundary element method volume conductor model», *Clin Neurophysiol*, vol. 113, fasc. 5, pp. 702–712, mag. 2002, doi: 10.1016/s1388-2457(02)00030-5.
[62] T. Medani, D. Lautru, D. Schwartz, Z. Ren, e G. Sou, «FEM Method for the EEG Forward Problem and Improvement Based on Modification of the Saint Venant's Method», *Progress in Electromagnetics Research*, vol. 153, pp. 11–22, ott. 2015, doi: 10.2528/PIER15050102.
[63] M. J. D. Cook e Z. J. Koles, «A high-resolution anisotropic finite-volume head model for EEG source analysis», *Conf Proc IEEE Eng Med Biol Soc*, vol. 2006, pp. 4536–4539, 2006, doi: 10.1109/IEMBS.2006.260314.
[64] F. Vatta, F. Meneghini, F. Esposito, S. Mininel, e F. Di Salle, «Solving the forward problem in EEG source analysis by spherical and fdm head modeling: a comparative analysis - biomed 2009», *Biomed Sci Instrum*, vol. 45, pp. 382–388, 2009.
[65] «The FieldTrip-SimBio pipeline for EEG forward solutions | BioMedical Engineering OnLine | Full Text». Consultato: 22 ottobre 2024. [Online]. Disponibile su: https://biomedical-engineering-online.biomedcentral.com/articles/10.1186/s12938-018-0463-y
[66] J. Vorwerk, M. Clerc, M. Burger, e C. H. Wolters, «Comparison of boundary element and finite element approaches to the EEG forward problem», *Biomed Tech (Berl)*, vol. 57 Suppl 1, p. /j/bmte.2012.57.issue-s1-O/bmt-2012-4152/bmt-2012-4152.xml, set. 2012, doi: 10.1515/bmt-2012-4152.
[67] J. Vorwerk, R. Oostenveld, M. C. Piastra, L. Magyari, e C. H. Wolters, «The FieldTrip-SimBio pipeline for EEG forward solutions», *BioMedical Engineering OnLine*, vol. 17, fasc. 1, p. 37, mar. 2018, doi: 10.1186/s12938-018-0463-y.
[68] F. Babiloni, F. Carducci, C. Babiloni, e A. Urbano, «Improved realistic Laplacian estimate of highly-sampled EEG potentials by regularization techniques», *Electroencephalogr Clin Neurophysiol*, vol. 106, fasc. 4, pp. 336–343, apr. 1998, doi: 10.1016/s0013-4694(97)00124-7.
[69] D.-W. Lim *et al.*, «Cerebral lateralization index based on intensity of bold signal of FMRI», *Int J Neurosci*, vol. 118, fasc. 11, pp. 1628–1642, nov. 2008, doi: 10.1080/00207450802330777.
[70] A. K. Liu, A. M. Dale, e J. W. Belliveau, «Monte Carlo simulation studies of EEG and MEG localization accuracy», *Hum Brain Mapp*, vol. 16, fasc. 1, pp. 47–62, mag. 2002, doi: 10.1002/hbm.10024.
[71] F.-H. Lin, T. Witzel, M. S. Hämäläinen, A. M. Dale, J. W. Belliveau, e S. M. Stufflebeam, «Spectral spatiotemporal imaging of cortical oscillations and interactions in the human brain», *NeuroImage*, vol. 23, fasc. 2, pp. 582–595, ott. 2004, doi: 10.1016/j.neuroimage.2004.04.027.
[72] L. M. Andersen, K. Jerbi, e S. S. Dalal, «Can EEG and MEG detect signals from the human cerebellum?», *NeuroImage*, vol. 215, p. 116817, lug. 2020, doi: 10.1016/j.neuroimage.2020.116817.

[73] A. Thielscher, A. Antunes, e G. B. Saturnino, «Field modeling for transcranial magnetic stimulation: A useful tool to understand the physiological effects of TMS?», in *2015 37th Annual International Conference of the IEEE Engineering in Medicine and Biology Society (EMBC)*, ago. 2015, pp. 222–225. doi: 10.1109/EMBC.2015.7318340.